

Recovering Stochastic Dynamics via Gaussian Schrödinger Bridges

Charlotte Bunne^{*1} Ya-Ping Hsieh^{*1} Marco Cuturi² Andreas Krause¹

Abstract

We propose a new framework to reconstruct a stochastic process $\{\mathbb{P}_t : t \in [0, T]\}$ using only samples from its *marginal* distributions, observed at start and end times 0 and T . This reconstruction is useful to infer population dynamics, a crucial challenge, e.g., when modeling the time-evolution of cell populations from single-cell sequencing data. Our general framework encompasses the more specific *Schrödinger bridge* (SB) problem, where \mathbb{P}_t represents the evolution of a thermodynamic system at almost equilibrium. Estimating such bridges is notoriously difficult, motivating our proposal for a novel adaptive scheme called the GSB_{FLOW}. Our goal is to rely on Gaussian approximations of the data to provide the reference stochastic process needed to estimate SB. To that end, we solve the SB problem with *Gaussian* marginals, for which we provide, as a central contribution, a closed-form solution and SDE-representation. We use these formulas to define the reference process used to estimate more complex SBs, and show that this does indeed help with its numerical solution. We obtain notable improvements when reconstructing both synthetic processes and single-cell genomics experiments.

1. Introduction

Problem formulation; major challenges. Let \mathbb{P}_t be a stochastic process on $[0, T]$ and let $\hat{\mathbb{P}}_0, \hat{\mathbb{P}}_T$ be two empirical distributions on \mathbb{R}^d . The goal of this paper is to:

Find a “suitable” \mathbb{P}_t such that $\mathbb{P}_0 \simeq \hat{\mathbb{P}}_0, \mathbb{P}_T \simeq \hat{\mathbb{P}}_T$. (\star)

Such problems have recently attracted significant attention in biology due to the advent of the *single-cell RNA sequencing* technique (Macosko et al., 2015), where $\hat{\mathbb{P}}_0$ and $\hat{\mathbb{P}}_T$ represent random samples of transcribed genes of a cell at

^{*}Equal contribution ¹Department of Computer Science, ETH Zurich ²Google Research (currently at Apple). Correspondence to: Charlotte Bunne <bunne@ethz.ch>, Ya-Ping Hsieh <yap-ing.hsieh@inf.ethz.ch>.

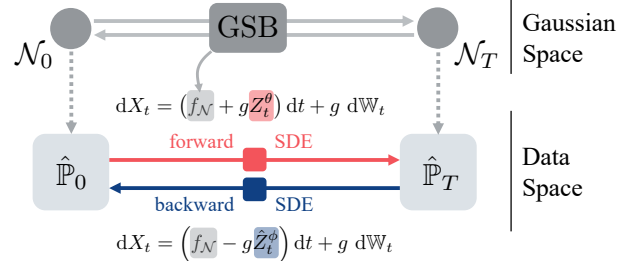


Figure 1. Solving the Schrödinger bridge (SB) problem between $\hat{\mathbb{P}}_0$ and $\hat{\mathbb{P}}_T$ is notoriously difficult, because it requires learning the time-dependent drifts of two SDEs that should recover the desired marginals, and a random initialization for these drifts is usually extremely far from satisfying that constraint. We propose a data-dependent procedure that relies first on Gaussian approximations of the data measures, which provide a closed-form drift f_N in (13) (the Gaussian SB). We show this facilitates next the training of forward/backward drift terms $\hat{Z}_t^\theta, \hat{Z}_t^\phi$.

time 0 and T . In this context, recovering the dynamics from $\hat{\mathbb{P}}_0$ to $\hat{\mathbb{P}}_T$ has extremely important scientific and biomedical implications (Kulkarni et al., 2019), such as understanding how and why tumor cells evade cancer therapies (Frangieh et al., 2021) or cell development (Schiebinger et al., 2019).

As stated, the problem (\star) is clearly ill-posed since we need further assumptions to provide meaningful criteria for the “suitability” of \mathbb{P}_t . Unfortunately, in most applications, notably biology, we often have little to no prior information about the underlying process \mathbb{P}_t (Liberali et al., 2014). To address these challenges, we draw inspiration from recent advances in a special case of (\star): generative modeling.

Generative models and Schrödinger bridges. When $\hat{\mathbb{P}}_T$ is a simple distribution, say $\mathcal{N}(0, I)$, our problem (\star) becomes the classical *generative modeling* task, which seeks to transform a noise distribution $\hat{\mathbb{P}}_T$ into a complex data distribution $\hat{\mathbb{P}}_0$. Recently, *score-based generative model* (SGM) (Sohl-Dickstein et al., 2015; Song and Ermon, 2019; Song et al., 2021), have shown practical success for this task, based on the key insight that it is easy to define a “reference process” \mathbb{Q}_t that transforms *any* data distribution $\hat{\mathbb{P}}_0$ into (almost) $\mathcal{N}(0, I)$. With such a reference process, solving (\star) corresponds to inverting \mathbb{Q}_t in time, for which many training procedures have been proposed (Song et al., 2021). Very recently, Chen et al. (2021a) and De Bortoli et al. (2021b)

discovered that SGMs can be seen as approximating an *KL-minimization* problem called the (generalized) *Schrödinger bridge* (SB) (Schrödinger, 1931; 1932)

$$\min_{\mathbb{P}_0=\hat{\mathbb{P}}_0, \mathbb{P}_T=\hat{\mathbb{P}}_T} D_{\text{KL}}(\mathbb{P}_t \parallel \mathbb{Q}_t), \quad (\text{SB})$$

where $\hat{\mathbb{P}}_0 \equiv p_{\text{data}}$ and $\hat{\mathbb{P}}_T = \mathcal{N}(0, I)$. Importantly, unlike other SGM interpretations, (SB) remains a reasonable objective for *arbitrary* $\hat{\mathbb{P}}_T$ once a ‘‘coarse approximation’’ \mathbb{Q}_t of \mathbb{P}_t is chosen. Such generality, nonetheless, comes at the price of being notoriously difficult to estimate due to a dilemma: Choosing an overly simple \mathbb{Q}_t in (SB), such as Brownian motions, presumes unrealistic dynamics of \mathbb{P}_t and leads to solutions with poor data-fit. On the other hand, to date, it is unclear how to design a more sophisticated \mathbb{Q}_t that takes data into account while retaining the necessary numerical efficiency of the simple dynamics.

Our contributions. In this paper, we resolve the above issues via constructing a *data-informed* reference process based on $\hat{\mathbb{P}}_0$ and $\hat{\mathbb{P}}_T$. We derive the *closed-form solutions* for a simpler variant of (SB) with *Gaussian* marginals

$$\mathbb{Q}_t^* := \operatorname{argmin}_{\mathbb{P}_0=\mathcal{N}_0, \mathbb{P}_T=\mathcal{N}_T} D_{\text{KL}}(\mathbb{P}_t \parallel Y_t), \quad (1)$$

where $\mathcal{N}_0, \mathcal{N}_T$ are two normal distributions with the same means and covariances as $\hat{\mathbb{P}}_0, \hat{\mathbb{P}}_T$, and Y_t is a wide class of *stochastic differential equations* (SDEs) that encompasses all widely-adopted reference processes for (SB). We then propose to learn (SB) with \mathbb{Q}_t replaced by \mathbb{Q}_t^* , since the latter embodies a variant of the ‘‘optimal process’’ when restricting attention to the first two moments of the data (see Fig. 1). To summarize, we make the following contributions:

1. As a central contribution, we derive closed-form expressions for the conditional probabilities and SDE representations of the *Gaussian Schrödinger bridge*, i.e., problems of the form (1). The proof combines a number of ideas from entropic optimal transport, Gaussian analysis, and generator theory, which might be of independent interest; see Section 3.2 for details.

2. We use \mathbb{Q}_t^* , the solution to (1), to attack (★) by solving

$$\min_{\mathbb{P}_0=\hat{\mathbb{P}}_0, \mathbb{P}_T=\hat{\mathbb{P}}_T} D_{\text{KL}}(\mathbb{P}_t \parallel \mathbb{Q}_t^*).$$

Based on our closed-form expressions of the conditional probabilities, we design an efficient *pretraining* routine to suitably initialize *both* the forward and backward drift functions, one carrying from $\hat{\mathbb{P}}_0$ to $\hat{\mathbb{P}}_T$ and the other from $\hat{\mathbb{P}}_T$ to $\hat{\mathbb{P}}_0$. In previous work (Chen et al., 2021a; De Bortoli et al., 2021b), only the backward pretraining is possible due to the fact that, in contrast to \mathbb{Q}_t^* , existing reference processes are completely data-oblivious.

3. We perform experiments on both synthetic and single-cell genomics data, and observe that the proposal process \mathbb{Q}_t^* along with the novel pretraining procedure significantly stabilizes the numerics of SB-based objectives. Notably,

on real datasets, our algorithm applied to the much harder task of mapping $\hat{\mathbb{P}}_0$ to $\hat{\mathbb{P}}_T$ achieves comparable Wasserstein loss to the state-of-the-art methods on generative modeling (i.e., learning from $\mathcal{N}(0, I)$ to $\hat{\mathbb{P}}_T$).

Related work. Several methods have been proposed to reconstruct deterministic paths between marginal distributions, building notably on optimal transport theory (Lavenant et al., 2021) or normalizing flows (Rezende and Mohamed, 2015), or even combining both (Tong et al., 2020; Huang et al., 2021a). These displacements can be parameterized by an energy function, solving the JKO scheme (Alvarez-Melis et al., 2021; Mokrov et al., 2021) or directly inferring it (Bunne et al., 2022), but they all adopt a deterministic formulation of OT which does not allow to sample paths agreeing with these marginals, but rather simply interpolate between them. The study of (SB) has only recently taken off in the learning literature, arising from rich mathematical foundations (Léonard, 2013; Chen et al., 2021b) to finding novel applications in generative modeling (Chen et al., 2021a; De Bortoli et al., 2021b; Vargas et al., 2021; Wang et al., 2021), sampling (Bernton et al., 2019; Huang et al., 2021c), and to estimate high-dimensional integrals (Pavon et al., 2021).

2. Background

Schrödinger bridge. The intuition behind the SB is best illustrated by the simple case where $\mathbb{Q}_t = \mathbb{W}_t$, which presupposes that the process \mathbb{P}_t we wish to reconstruct behaves as a physical system in thermal equilibrium. By the Gaussian increments of \mathbb{W}_t , for any marginal $\hat{\mathbb{P}}_0$ at time 0, \mathbb{W}_t would predict the distribution at time T to be $\hat{\mathbb{P}}_0 * \mathcal{N}(0, T \cdot I)$ where $*$ denotes the convolution operator. If this distribution differs from the actual data $\hat{\mathbb{P}}_T$, then \mathbb{P}_t must also differ from \mathbb{W}_t . To find out \mathbb{P}_t , Schrödinger (1931; 1932) considers the objective (SB) as the ‘‘most likely process’’ that explains the marginal distributions $\hat{\mathbb{P}}_0, \hat{\mathbb{P}}_T$ relative to \mathbb{W}_t . This idea generalizes verbatim to any reference process \mathbb{Q}_t .

In practice, \mathbb{Q}_t is taken to be the measure of an SDE with drift and scale,

$$dY_t = f(t, Y_t) dt + g(t) d\mathbb{W}_t \equiv f dt + g d\mathbb{W}_t \quad (2)$$

with some initial condition Y_0 . In this case, it turns out that the solution to (SB) is itself given by two coupled SDEs of the form (Léonard, 2013)

$$dX_t = (f + gZ_t) dt + g d\mathbb{W}_t, \quad X_0 \sim \hat{\mathbb{P}}_0, \quad (3a)$$

$$dX_t = (f - g\hat{Z}_t) dt + g d\mathbb{W}_t, \quad X_T \sim \hat{\mathbb{P}}_T, \quad (3b)$$

where $Z_t, \hat{Z}_t: \mathbb{R}^d \rightarrow \mathbb{R}^d$ are two time-indexed smooth *vector fields* called the optimal forward and backward drift, respectively, and (3b) runs backward in time (i.e., from $T \rightarrow 0$). If we parametrize the forward drift by $Z_t^\theta(x)$ and the backward drift by $\hat{Z}_t^\phi(x)$ with some parameters θ, ϕ , then the negative likelihood function for θ and ϕ can be

expressed as (Chen et al., 2021a)

$$\ell(x_0; \phi) = \int_0^T \mathbb{E}_{(3a)} \left[\frac{1}{2} \|\hat{Z}_t^\phi\|^2 + g \nabla_x \cdot \hat{Z}_t^\phi + \langle Z_t^\theta, \hat{Z}_t^\phi \rangle dt \middle| X_0 = x_0 \right], \quad (4a)$$

$$\ell(x_T; \theta) = \int_0^T \mathbb{E}_{(3b)} \left[\frac{1}{2} \|Z_t^\theta\|^2 + g \nabla_x \cdot Z_t^\theta + \langle \hat{Z}_t^\phi, Z_t^\theta \rangle dt \middle| X_T = x_T \right], \quad (4b)$$

where $\nabla_x \cdot$ denotes the divergence operator w.r.t. the x variable: For any $v: \mathbb{R}^d \rightarrow \mathbb{R}^d$, $\nabla_x \cdot v(x) := \sum_{i=1}^d \frac{\partial}{\partial x_i} v_i(x)$.

SGMs and pretraining of (SB). Evaluating the negative likelihood $\ell(x_0; \phi)$ involves simulating the SDE (3a) with a general drift function $Z_t^\theta(x)$, which is an expensive operation. However, if $Z_t \equiv 0$, then the *conditional distribution* $X_t | X_0 = x_0$ of (3a) often admits a closed-form expression since it merely simulates the reference SDE Y_t . For this reason, previous work on solving (SB) (Chen et al., 2021a) propose to initialize θ_0 such that $Z_t^{\theta_0}(\cdot) \equiv 0$ (for instance, $Z_t^{\theta_0}(\cdot)$ being a neural network with zero output weights), and train the backward drift $\hat{Z}_t^\phi(x)$ first. This is called *pretraining* in the literature, and has proved to be of central importance in the empirical performance of (SB) for generative modelling. In our experiments, we continue to observe the substantial benefit of pretraining when both $\hat{\mathbb{P}}_0$ and $\hat{\mathbb{P}}_T$ are complicated distributions.

3. Closed-Form Solutions of Gaussian Schrödinger Bridges

In this section, we present the closed-form solutions of *Gaussian Schrödinger bridges* (GSBs):

$$\min_{\mathbb{P}_0 = \mathcal{N}_0, \mathbb{P}_T = \mathcal{N}_T} D_{\text{KL}}(\mathbb{P}_t \| \mathbb{Q}_t) \quad (\text{SB}_{\mathcal{N}})$$

where \mathcal{N}_0 and \mathcal{N}_T are normally distributed with arbitrary means and covariances. We work with a general class of reference SDEs introduced in Section 3.1. Section 3.2 contains the statements of the main theorems. Important instances of our theory are presented in Section 3.3, and Section 3.4 discusses how our theorems generalize prior results.

3.1. Linear Stochastic Differential Equations

We take the reference process \mathbb{Q}_t in $(\text{SB}_{\mathcal{N}})$ to be a *linear* SDE, with some initial condition Y_0 :

$$dY_t = (c(t)Y_t + \alpha(t)) dt + g(t) d\mathbb{W}_t \quad (5)$$

Here, $c(t): \mathbb{R}^+ \rightarrow \mathbb{R}$, $\alpha(t): \mathbb{R}^+ \rightarrow \mathbb{R}^d$, and $g(t): \mathbb{R}^+ \rightarrow \mathbb{R}^+$ are smooth functions. It is well-known that the solution to (5) is (Platen and Bruti-Liberati, 2010):

$$Y_t = \tau_t \left(Y_0 + \int_0^t \tau_s^{-1} \alpha(s) ds + \int_0^t \tau_s^{-1} g(s) d\mathbb{W}_s \right) \quad (6)$$

where $\tau_t := \exp\left(\int_0^t c(s) ds\right)$.

A crucial fact in our analysis is that Y_t is a *Gaussian process* given any Y_0 , and is thus characterized by the first two moments. Using the independent increments of \mathbb{W}_t and Itô's isometry (Protter, 2005), we compute:

$$\mathbb{E}[Y_t | Y_0] = \tau_t \left(Y_0 + \int_0^t \tau_s^{-1} \alpha(s) ds \right) =: \eta(t) \quad (7)$$

and, for any $t' \geq t$,

$$\begin{aligned} & \mathbb{E} \left[(Y_t - \eta(t))(Y_{t'} - \eta(t'))^\top \middle| Y_0 \right] \\ &= \left(\tau_t \tau_{t'} \int_0^t \tau_s^{-2} g^2(s) ds \right) I =: \kappa(t, t') I. \end{aligned} \quad (8)$$

3.2. Main Results

Let $\mathcal{N}_0 = \mathcal{N}(\mu_0, \Sigma_0)$ and $\mathcal{N}_T = \mathcal{N}(\mu_T, \Sigma_T)$ be two arbitrary Gaussian distributions in $(\text{SB}_{\mathcal{N}})$. We will adopt the following notation from Janati et al. (2020):

$$\begin{aligned} D_\sigma &:= \left(4\Sigma_0^{\frac{1}{2}} \Sigma_T \Sigma_0^{\frac{1}{2}} + \sigma^4 I \right)^{\frac{1}{2}}, \\ C_\sigma &:= \frac{1}{2} \left(\Sigma_0^{\frac{1}{2}} D_\sigma \Sigma_0^{-\frac{1}{2}} - \sigma^2 I \right), \end{aligned}$$

where $\sigma > 0$ is to be determined later. Our main result in this section is:

Theorem 1. Denote by \mathbb{P}_t^* the solution to $(\text{SB}_{\mathcal{N}})$. Set

$$r_t := \frac{\kappa(t, T)}{\kappa(T, T)}, \quad \bar{r}_t := \tau_t - r_t \tau_T, \quad \sigma_\star := \sqrt{\tau_T^{-1} \kappa(T, T)},$$

$$\zeta(t) := \tau_t \int_0^t \tau_s^{-1} \alpha(s) ds, \quad \rho_t := \frac{\int_0^t \tau_s^{-2} g^2(s) ds}{\int_0^T \tau_s^{-2} g^2(s) ds},$$

$$P_t := \dot{r}_t (r_t \Sigma_T + \bar{r}_t C_{\sigma_\star}), \quad Q_t := -\dot{\bar{r}}_t (\bar{r}_t \Sigma_0 + r_t C_{\sigma_\star}),$$

$$S_t := P_t - Q_t^\top + [c(t)\kappa(t, t)(1 - \rho_t) - g^2(t)\rho_t] I. \quad (9)$$

Then the following holds:

1. The solution \mathbb{P}_t^* is a Markov Gaussian process whose marginal variable X_t^* follows $\mathcal{N}(\mu_t^*, \Sigma_t^*)$, where

$$\mu_t^* := \bar{r}_t \mu_0 + r_t \mu_T + \zeta(t) - r_t \zeta(T), \quad (10)$$

$$\begin{aligned} \Sigma_t^* &:= \bar{r}_t^2 \Sigma_0 + r_t^2 \Sigma_T + r_t \bar{r}_t (C_{\sigma_\star} + C_{\sigma_\star}^\top) \\ &\quad + \kappa(t, t)(1 - \rho_t) I. \end{aligned} \quad (11)$$

2. X_t^* admits a closed-form solution as the SDE:

$$dX_t^* = f_{\mathcal{N}}(t, X_t^*) dt + g(t) d\mathbb{W}_t \quad (12)$$

where

$$f_{\mathcal{N}}(t, x) := S_t^\top \Sigma_t^{*-1} (x - \mu_t^*) + \dot{\mu}_t^*. \quad (13)$$

Moreover, the matrix $S_t^\top \Sigma_t^{*-1}$ is symmetric.

Proof sketch. The full proof can be found in Appendix A.2, which builds essentially on the following ideas:

1. Leveraging existing results (Bojilov and Galichon, 2016; del Barrio and Loubes, 2020; Janati et al., 2020; Mallasto et al., 2021), we first solve an appropriately chosen *static* GSB determined by the reference process \mathbb{Q}_t .
2. It can be shown from the disintegration formula

Recovering Stochastic Dynamics via Gaussian Schrödinger Bridges

SDE WITH $\alpha(t) \equiv 0$	SETTING	$\kappa(t, t')$	σ_\star^2	r_t	\bar{r}_t	ρ_t	$\zeta(t)$
BM	$c(t) \equiv 0$ $g(t) \equiv \omega \in \mathbb{R}^+$	$\omega^2 t$	$\omega^2 T$	$\frac{t}{T}$	$1 - \frac{t}{T}$	$\frac{t}{T}$	0
VE SDE	$c(t) \equiv 0$ $g(t) = \sqrt{\hat{q}(t)}$	$q(t)$	$q(T)$	$\frac{q(t)}{q(T)}$	$1 - \frac{q(t)}{q(T)}$	$\frac{q(t)}{q(T)}$	0
VP SDE	$-2c(t) = g^2(t)$	$\tau_{t'}(\tau_t^{-1} - \tau_t)$	$\tau_T^{-1} - \tau_T$	$\frac{\tau_t^{-1} - \tau_t}{\tau_T^{-1} - \tau_T}$	$\tau_T \left(\frac{\tau_t}{\tau_T} - \frac{\tau_t^{-1} - \tau_t}{\tau_T^{-1} - \tau_T} \right)$	$\frac{\tau_t^{-1}(\tau_t^{-1} - \tau_t)}{\tau_T^{-1}(\tau_T^{-1} - \tau_T)}$	0
SUB-VP SDE	$\frac{g^2(t)}{-2c(t)} = 1 - \tau_t^4$	$\tau_t \tau_{t'} (\tau_t^{-1} - \tau_t)^2$	$\tau_T (\tau_T^{-1} - \tau_T)^2$	$\frac{\tau_t}{\tau_T} \cdot \left(\frac{\tau_t^{-1} - \tau_t}{\tau_T^{-1} - \tau_T} \right)^2$	$\tau_t \left(1 - \left(\frac{\tau_t^{-1} - \tau_t}{\tau_T^{-1} - \tau_T} \right)^2 \right)$	$\left(\frac{\tau_t^{-1} - \tau_t}{\tau_T^{-1} - \tau_T} \right)^2$	0

SDE WITH $\alpha(t) \neq 0$	SETTING	$\kappa(t, t')$	σ_\star^2	r_t	\bar{r}_t	ρ_t	$\zeta(t)$
OU/VASICEK	$c(t) \equiv -\lambda \in \mathbb{R}$ $\alpha(t) \equiv \mathbf{v} \in \mathbb{R}^d$ $g(t) \equiv \omega \in \mathbb{R}^+$	$\frac{\omega^2 e^{-\lambda t'} \sinh \lambda t}{\lambda}$	$\frac{\omega^2 \sinh \lambda T}{\lambda}$	$\frac{\sinh \lambda t}{\sinh \lambda T}$	$\sinh \lambda t \coth \lambda T$ $-\sinh \lambda t \coth \lambda T$	$e^{-\lambda(T-t)}$ $\frac{\sinh \lambda t}{\sinh \lambda T}$	$\frac{\mathbf{v}}{\lambda} (1 - e^{-\lambda t})$
$\alpha(t)$ -BDT	$c(t) \equiv 0$ $g(t) \equiv \omega \in \mathbb{R}^+$	$\omega^2 t$	$\omega^2 T$	$\frac{t}{T}$	$1 - \frac{t}{T}$	$\frac{t}{T}$	$\int_0^t \alpha(s) ds$

Table 1. Examples of SDEs and the functions relevant to the closed-form solutions of $(\text{SB}_{\mathcal{N}})$.

(Léonard, 2013), the solution of the static GSBs, and properties of (6) that \mathbb{P}_t^\star is a Markov Gaussian process with mean (10) and covariance (11).

- Invoking the *generator theory* (Protter, 2005), to prove (12), it suffices to show that X_t^\star satisfies, for any sufficiently regular test function $u : \mathbb{R}^+ \times \mathbb{R}^d \rightarrow \mathbb{R}$,

$$\lim_{h \rightarrow 0} \frac{\mathbb{E}[u(t+h, X_{t+h}^\star) \mid X_t^\star = x]}{h} = \mathcal{L}_t u(t, x), \quad (14)$$

where

$$\begin{aligned} \mathcal{L}_t u(t, x) := & \frac{\partial}{\partial t} u(t, x) \\ & + \frac{g^2(t)}{2} \Delta u(t, x) + \langle \nabla u(t, x), f_{\mathcal{N}}(t, x) \rangle \end{aligned} \quad (15)$$

is the generator for the process (12).

- Since the marginal/joint/conditional distributions of a Gaussian process are still Gaussian, the expectation in (14) requires to express Gaussian integrals as differential operators. To this end, the appropriate tool is the ‘‘central identity in quantum field theory’’ (Zee, 2010).
- Proof concludes by matching terms in (14) and (15). \square

As an immediate corollary of Theorem 1, we obtain the closed-form expressions for conditional marginals of X_t^\star . Importantly, this will allow us to perform a *pretraining* procedure, described in detail in Section 4, for *both* the forward and the backward drifts, which will prove extremely valuable in practice.

Corollary 1. *Let $X_t^\star \sim \mathbb{P}_t^\star$ be the the solution to $(\text{SB}_{\mathcal{N}})$. Then the conditional distribution of X_t^\star given end points has*

a simple solution: $X_t^\star \mid X_0^\star = x_0 \sim \mathcal{N}(\mu_{t|0}^\star, \Sigma_{t|0}^\star)$, where

$$\begin{aligned} \mu_{t|0}^\star &= \bar{r}_t x_0 + r_t (\mu_T + C_{\sigma_\star}^\top \Sigma_0^{-1} (x_0 - \mu_0)) + \zeta(t) - r_t \zeta(T) \\ &= \bar{r}_t x_0 + r_t \mu_{T|0}^\star + \zeta(t) - r_t \zeta(T), \end{aligned} \quad (16)$$

$$\begin{aligned} \Sigma_{t|0}^\star &= r_t^2 (\Sigma_T - C_{\sigma_\star}^\top \Sigma_0^{-1} C_{\sigma_\star}) + \kappa(t, t) (1 - \rho_t) I \\ &= r_t^2 \Sigma_{T|0}^\star + \kappa(t, t) (1 - \rho_t) I. \end{aligned} \quad (17)$$

Similarly, $X_t^\star \mid X_T^\star = x_T \sim \mathcal{N}(\mu_{t|T}^\star, \Sigma_{t|T}^\star)$, where

$$\begin{aligned} \mu_{t|T}^\star &= r_t x_T + \bar{r}_t (\mu_0 + C_{\sigma_\star} \Sigma_T^{-1} (x_T - \mu_T)) + \zeta(t) - r_t \zeta(T) \\ &= r_t x_T + \bar{r}_t \mu_{0|T}^\star + \zeta(t) - r_t \zeta(T), \end{aligned} \quad (18)$$

$$\begin{aligned} \Sigma_{t|T}^\star &= \bar{r}_t^2 (\Sigma_0 - C_{\sigma_\star} \Sigma_T^{-1} C_{\sigma_\star}^\top) + \kappa(t, t) (1 - \rho_t) I \\ &= \bar{r}_t^2 \Sigma_{0|T}^\star + \kappa(t, t) (1 - \rho_t) I. \end{aligned} \quad (19)$$

The proof is a straightforward combination of (A.21), Lemma A.3, and (10)–(11).

3.3. Examples

Our framework captures most popular reference SDEs in the generative modeling literature as well as other mathematical models for learning single-cell dynamics. A non-exhaustive list includes (see Table 1 for details):

- The basic *Brownian motion* (BM) and the *Ornstein–Uhlenbeck* (OU) processes, both widely adopted as the reference process for SB-based models (De Bortoli et al., 2021a;b; Lavenant et al., 2021; Vargas et al., 2021; Wang et al., 2021).
- The *variance exploding SDEs* (VE SDEs), which underlies the training of *score matching with Langevin*

dynamics (Song and Ermon, 2019; Song et al., 2021; Huang et al., 2021b).

- The *variance preserving SDEs* (VP SDEs), which can be seen as the continuous limit of *denoising diffusion probabilistic models* (Sohl-Dickstein et al., 2015; Ho et al., 2020; Song et al., 2021).
- The *sub-VP SDEs* proposed by Song et al. (2021), which are motivated by reducing the variance of VP SDEs.
- Several important SDEs in financial engineering, such as the *Vasicek model* (which generalizes OU processes) and the *constant volatility $\alpha(t)$ -Black–Derman–Toy* (BDT) model (Platen and Bruti-Liberati, 2010).

3.4. Comparison with Existing Work

To our knowledge, all results in [Theorem 1](#) are novel, with the sole exception of a degenerate case for (11) ($c(t) \equiv \alpha(t) \equiv 0$ and $g(t) \equiv \text{const.}$), which appears in the prior work of Mallasto et al. (2021). In the above degenerate setting, and if we additionally assume $\mu_0 = \mu_T = 0$, then it is perhaps possible to extend the calculations in (Mallasto et al., 2021, (43)-(56)) to derive a different formula for $f_{\mathcal{N}}(t, x)$. However, these calculations involve first “guessing” the right solution, and then verifying by (rather tedious) reverse-engineering, which already faces challenges when $\mu_0 \neq \mu_T$. The symmetry of the matrix $S_t^\top \Sigma_t^{*-1}$, on the other hand, seems beyond the reach of an educated guess, let alone (13) for the general class of \mathbb{Q}_t we consider.

A stochastic control problem related to $(\text{SB}_{\mathcal{N}})$ is studied by Chen et al. (2015; 2016). The key difference between our work and their approaches is that the optimal control derived therein (which corresponds to our $f_{\mathcal{N}}(t, x)$ in (13)) is expressed in terms of the solution to a matrix Riccati equation with convoluted boundary conditions; see (Chen et al., 2016, (50)-(53)). In contrast, our solutions in [Theorem 1](#) are explicitly expressed in terms of the inputs $\mu_0, \mu_T, \Sigma_0, \Sigma_T$, which are amenable to efficient implementation.

4. Dynamics Reconstruction via GSBFLOW

Building on the closed-form solutions in [Section 3](#), we present an end-to-end learning paradigm that takes two marginal distributions $\hat{\mathbb{P}}_0, \hat{\mathbb{P}}_T$ to output the reconstruction of the underlying stochastic dynamics \mathbb{P}_t . Because our framework relies on GSB, we call our algorithm the **GSBFLOW**.

Step 1: Moment estimates and GSB initialization. We first compute the means μ_0, μ_T and covariances Σ_0, Σ_T of the input distributions, and plug them into (13) and (16)-(19). Note that these computations are done only *once* for every dataset, and can be reused for all subsequent training.

Step 2: Forward and backward pretraining. Denoting by \mathbb{Q}_t^* the measure of $f_{\mathcal{N}} dt + g d\mathbb{W}_t$ in (13), we propose

Algorithm 1 Forward and Backward Pretraining

Input: Marginal distributions $\hat{\mathbb{P}}_0, \hat{\mathbb{P}}_T$, initial parameters $\tilde{\theta}_0, \tilde{\phi}_0$ such that $Z_t^{\tilde{\theta}_0}(\cdot) = \hat{Z}_t^{\tilde{\phi}_0}(\cdot) \equiv 0$, iteration counts K_θ, K_ϕ , learning rates $\gamma_\theta, \gamma_\phi$

Output: Pretrained parameters θ_0, ϕ_0

Initialize $\theta_0 \leftarrow \tilde{\theta}_0, \phi_0 \leftarrow \tilde{\phi}_0$.

for $k = 1$ **to** K_ϕ **do**

Sample X_t from (16)-(17) with $x_0 \sim \hat{\mathbb{P}}_0$

Compute $\ell(x_0; \phi)$ via (22a)

Update $\phi_0 \leftarrow \phi_0 - \gamma_\phi \nabla \ell(x_0; \phi_0)$

for $k = 1$ **to** K_θ **do**

Sample X_t from (18)-(19) with $x_T \sim \hat{\mathbb{P}}_T$

Compute $\ell(x_T; \theta)$ via (22b)

Update $\theta_0 \leftarrow \theta_0 - \gamma_\theta \nabla \ell(x_T; \theta_0)$

Algorithm 2 GSBFLOW

Input: Marginal distributions $\hat{\mathbb{P}}_0, \hat{\mathbb{P}}_T$, pretrained parameters θ_0, ϕ_0 , caching frequency M , iteration counts $K_{\text{in}}, K_{\text{out}}$, learning rates $\gamma_\theta, \gamma_\phi$

Output: Optimal forward and backward drifts $Z_t(\cdot), \hat{Z}_t(\cdot)$ for (20)

Initialize $\theta \leftarrow \theta_0, \phi \leftarrow \phi_0$.

for $k = 1$ **to** K_{out} **do**

for $j = 1$ **to** K_{in} **do**

if $j \bmod M = 0$ **then**

Simulate (21a) with $x_0 \sim \hat{\mathbb{P}}_0$

Compute $\ell(x_0; \phi)$ via (22a)

Update $\phi \leftarrow \phi - \gamma_\phi \nabla \ell(x_0; \phi)$

for $j = 1$ **to** K_{in} **do**

if $j \bmod M = 0$ **then**

Simulate (21b) with $x_T \sim \hat{\mathbb{P}}_T$

Compute $\ell(x_T; \theta)$ via (22b)

Update $\theta \leftarrow \theta - \gamma_\theta \nabla \ell(x_T; \theta)$

to minimize the objective

$$\min_{\mathbb{P}_0 = \hat{\mathbb{P}}_0, \mathbb{P}_T = \hat{\mathbb{P}}_T} D_{\text{KL}}(\mathbb{P}_t \| \mathbb{Q}_t^*). \quad (20)$$

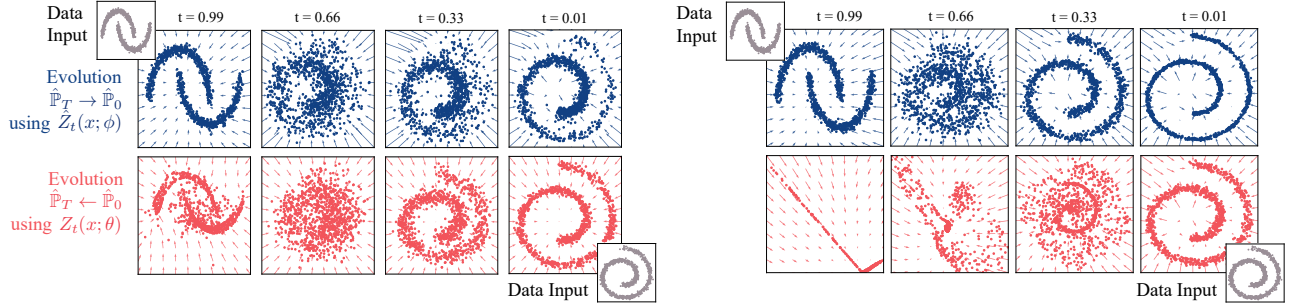
Following (3a)-(3b), we see that the optimal solution to (20) is given by two SDEs of the form:

$$dX_t = (f_{\mathcal{N}} + gZ_t) dt + g d\mathbb{W}_t, \quad X_0 \sim \hat{\mathbb{P}}_0, \quad (21a)$$

$$dX_t = (f_{\mathcal{N}} - g\hat{Z}_t) dt + g d\mathbb{W}_t, \quad X_T \sim \hat{\mathbb{P}}_T, \quad (21b)$$

where (21b) runs backward in time. After parameterizing Z_t and \hat{Z}_t by two neural networks $Z_t^\theta(x), \hat{Z}_t^\phi(x)$ with parameters θ, ϕ , the corresponding negative likelihood in [Section 2](#) becomes

$$\ell(x_0; \phi) = \int_0^T \mathbb{E}_{(21a)} \left[\frac{1}{2} \|\hat{Z}_t^\phi\|^2 + g \nabla_x \cdot \hat{Z}_t^\phi + \langle Z_t^\theta, \hat{Z}_t^\phi \rangle dt \middle| X_0 = x_0 \right], \quad (22a)$$



(a) GSBFLOW with VE SDE.

(b) Chen et al. (2021a) with VE SDE.

Figure 2. Illustration of the time-dependent drifts learned by GSBFLOW compared to those recovered by the method proposed by Chen et al. (2021a) for two toy marginal distributions. *Top.* Evolution of $\hat{\mathbb{P}}_T$ (moons) \rightarrow $\hat{\mathbb{P}}_0$ (spiral) via backward policy $\hat{Z}_t^\phi(x)$. *Bottom.* Evolution of $\hat{\mathbb{P}}_0$ (spiral) \rightarrow $\hat{\mathbb{P}}_T$ (moons) via forward policy $\hat{Z}_t^\theta(x)$.

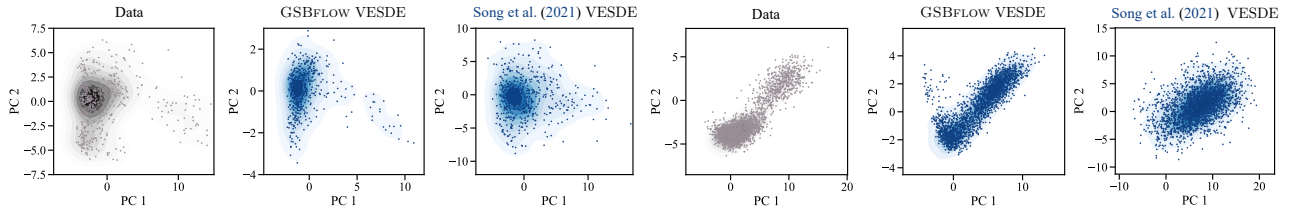


Figure 3. Visual evaluation of the ability of our method to model the generation of data from Moon et al. (2019) (left plots) and Schiebinger et al. (2019) (right plots), using density plots in 2D PCA space of generated points using either GSBFLOW (our method) or the procedure in Chen et al. (2021a).

$$\ell(x_T; \theta) = \int_0^T \mathbb{E}_{(21b)} \left[\frac{1}{2} \|Z_t^\theta\|^2 + g \nabla_x \cdot Z_t^\theta + \langle \hat{Z}_t^\phi, Z_t^\theta \rangle dt \middle| X_T = x_T \right]. \quad (22b)$$

Following existing work on training SB-based objectives (Chen et al., 2021a; De Bortoli et al., 2021b), we propose to initialize $\hat{\theta}_0, \hat{\phi}_0$ such that $Z_t^{\hat{\theta}_0}(x), \hat{Z}_t^{\hat{\phi}_0}(x) \equiv 0$, which can be easily achieved by zeroing out the last layer of the corresponding neural networks. In this case, estimating the conditional expectations in both (22a)-(22b) reduces to simulating (13) *conditioned* on the given start or end data points. Thanks to our closed-form expressions, this can be easily achieved by drawing Gaussian variables with mean and covariance prescribed in (21a)-(21b). The pretraining procedure is summarized in Algorithm 1.

Step 3: Alternating minimization. After the pretraining phase, we switch to minimizing (22a)-(22b) with general drifts in (21a)-(21b). We carry out this step in an alternating fashion: Since the bottleneck of our framework is to simulate the trajectories of SDEs, we perform several gradient updates for one parameter before drawing another batch of samples. See Algorithm 2 for a summary.

5. Experiments

The purpose of our experiments is to demonstrate that by leveraging second order moment information, GSBFLOW is significantly more stable compared to other SB-based objectives, specially when moving beyond the assumption that $\hat{\mathbb{P}}_T$ is a simple Gaussian. Indeed, while performing competitively in the generative setting ($\mathcal{N}_0 \rightarrow \hat{\mathbb{P}}_T$), our method *outperforms* when modeling the evolution of two complex distributions ($\hat{\mathbb{P}}_0 \rightarrow \hat{\mathbb{P}}_T$), the most general and ambitious setting to estimate a bridge, as shown on synthetic data and high-dimensional single-cell differentiation processes.

5.1. Synthetic Dynamics

The first task involves the evolution of two-dimensional synthetic data containing two interleaving half circles ($\hat{\mathbb{P}}_T$) into a spiral ($\hat{\mathbb{P}}_0$). We hereby evaluate both learned policies modeled via the forward $\hat{Z}_t^\theta(x)$ and backward score model $\hat{Z}_t^\phi(x)$, which construct a vector field progressively transporting samples from $\hat{\mathbb{P}}_0 \rightarrow \hat{\mathbb{P}}_T$ and $\hat{\mathbb{P}}_T \rightarrow \hat{\mathbb{P}}_0$, respectively. The solutions of the SDEs (21a)-(21b) are approximated using the Euler-Maruyama method given initial data inputs. Figure 2 shows the trajectories learned by GSBFLOW as well as previous work by Chen et al. (2021a), both based on VE SDEs (see Table 1 and Appendix D.1). We defer the results on other SDEs to Appendix B.

Table 2. Evaluation of predictive performance w.r.t. the entropy-regularized Wasserstein distance W_ϵ (Cuturi, 2013) of GSBFLOW and baselines on different single-cell datasets (using 3 runs).

Method	Tasks					
	Generation ($\mathcal{N}_0 \rightarrow \hat{\mathbb{P}}_T$) Wasserstein Loss $W_\epsilon \downarrow$		Evolution ($\hat{\mathbb{P}}_0 \rightarrow \hat{\mathbb{P}}_T$) Wasserstein Loss $W_\epsilon \downarrow$			
	Moon et al. 2019	Schiebinger et al. 2019	Moon et al. 2019	Schiebinger et al. 2019	Moon et al. (2019) (scaled)	Schiebinger et al. (2019) (scaled)
Chen et al. (2021a)						
VESDE	20.83 \pm 0.18	40.81 \pm 0.42	45.01 \pm 2.74	62.13 \pm 3.81	Num. Inst. ¹	Num. Inst. ¹
sub-VPSDE	19.96 \pm 0.58	48.15 \pm 3.38	59.15 \pm 44.08	Num. Inst. ¹	Num. Inst. ¹	Num. Inst. ¹
GSBFLOW (ours)						
VESDE	25.18 \pm 0.10	27.85 \pm 0.68	43.39 \pm 0.93	59.99 \pm 1.73	40.64 \pm 1.18	58.55 \pm 1.07

¹No predictions available due to numerical instabilities.

While in generative modeling, or, more concretely, in score-based modeling it is sufficient to parameterize only a single policy ($\hat{Z}_t^\phi(x)$), the task of learning to evolve $\hat{\mathbb{P}}_0$ into $\hat{\mathbb{P}}_T$ (Algorithm 2), requires one to recover *both* vector fields $\hat{Z}_t^\phi(x)$ and $Z_t^\theta(x)$. In simple setups such as the one considered here, previous SB-based methods (Chen et al., 2021a; De Bortoli et al., 2021b) are able to recover $\hat{Z}_t^\phi(x)$ by moving the synthetic population into a standard Gaussian ($t = 0.66$ in Fig. 2b) since the diffusion term $g \, d\mathbb{W}_s$ in (3a) consistently injects isotropic noise, thus recovering the standard generative modeling problem $\mathcal{N}_0 \rightarrow \hat{\mathbb{P}}_T$, which they are able to solve (see Fig. 2b). They fail, however, to recover the forward policy $Z_t^\theta(x)$. While this shortcut is feasible in low-dimensional data regimes, it gives rise to numerical instabilities and malfunctions when we move to more complex problems. As demonstrated in Fig. 2a, GSBFLOW is able to successfully learn both policies $Z_t^\theta(x)$ and $\hat{Z}_t^\phi(x)$ and reliably recovers the corresponding targets of the forward and backward evolutionary processes.

5.2. Single-Cell Dynamics

Single cell profiling technologies are able to provide rich feature representations (gene expression) of *individual* cells at any development state. A crucial issue that arises with such datasets is that the same cell cannot be measured twice. As a result, independent samples are collected at each snapshot, with no access to ground-truth single-cell trajectories, resulting in challenging, *unaligned*, datasets.

We investigate the ability of GSBFLOW to predict the evolution of such molecular processes ($\hat{\mathbb{P}}_0 \rightarrow \hat{\mathbb{P}}_T$), i.e., the inference of cell populations $\hat{\mathbb{P}}_T$ resulting from the developmental process of an initial cell population $\hat{\mathbb{P}}_0$, with the goal of learning individual dynamics, identify ancestor and descendant cells, and get a better understanding of biological differentiation. Besides studying $\hat{\mathbb{P}}_0 \rightarrow \hat{\mathbb{P}}_T$, we also test GSBFLOW on the task of learning an entire single-

cell landscape, and generate populations $\hat{\mathbb{P}}_T$ from noise \mathcal{N}_0 ($\mathcal{N}_0 \rightarrow \hat{\mathbb{P}}_T$). We consider the development of human embryonic stem cells (ESCs) grown as embryoid bodies into diverse cell lineages monitored by single-cell RNA sequencing methods (Moon et al., 2019) as well as reprogramming mouse embryonic fibroblasts (MEFs) into induced pluripotent stem cells (iPSCs) (Schiebinger et al., 2019). The evaluation is conducted on the first 20 or 30 components of the PCA space of the > 1500 highly differentiable genes (see Figs. 7–8). See Appendix C for details.

Learning to generate $\mathcal{N}_0 \rightarrow \hat{\mathbb{P}}_T$. The first experiment is the generative modeling setup which seeks to learn the underlying differentiation landscape from time-resolved scRNA-seq data jointly over all time points. For both tasks, the embryoid body differentiation as well as reprogramming MEFs into iPSC, we aim at learning $\hat{\mathbb{P}}_T$ from noise \mathcal{N}_0 . We compare GSBFLOW with state-of-the-art score-based generative models (Song et al., 2021) with VE SDEs and sub-VP SDEs in the backend. In this setting, $Z_t^\theta(x) = 0$. After training of $\hat{Z}_t^\phi(x)$, we are able to generate cell population samples by solving the reverse-time SDE (21b)—or (3b) for (Song et al., 2021)—using the Euler-Maruyama method. We evaluate the quality of the generated cellular states through distributional distances, i.e., the entropy-regularized Wasserstein distance W_ϵ (see Table 2) and by visualizing the first two principal components (PC), see Fig. 3. GSBFLOW performs competitively on reconstructing embryoid body differentiation landscapes (Moon et al., 2019), and outperforms score-based generative models baselines on the iPSC reprogramming task (Schiebinger et al., 2019) as quantified by W_ϵ between data and predictions.

Learning to evolve $\hat{\mathbb{P}}_0 \rightarrow \hat{\mathbb{P}}_T$. Besides being able to generate $\hat{\mathbb{P}}_T$ from noise, resolving and dissecting temporal dependencies and ancestor-descendant relationships is key for the understanding of biological processes. In the following, we thus analyze GSBFLOW’s ability to predict the temporal

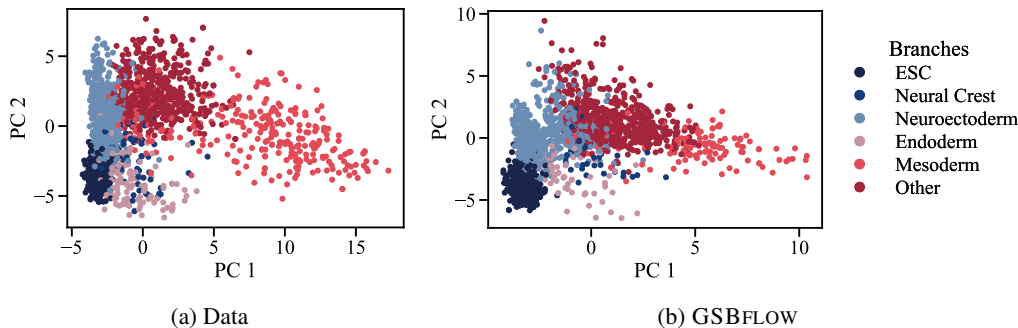


Figure 4. PCA embedding of the (a) Moon et al. (2019) data and (b) the GSBFLOW predictions colored by the lineage branch class.

evolution of populations governed by complex underlying dynamics. For the embryoid body differentiation (Moon et al., 2019), cells measured at day 1 to 3 serve as samples of $\hat{\mathbb{P}}_0$, while $\hat{\mathbb{P}}_T$ is constructed from samples between day 12 to 27. For the task of MEF reprogramming (Schiebinger et al., 2019), $\hat{\mathbb{P}}_0$ consists of cells in the initial stage of the differentiation process, i.e., day 1 to 3, and $\hat{\mathbb{P}}_T$ of cells in final states, i.e., day 15 to 18. As no ground truth trajectories are available in the data, we measure the correctness of the predictions at each time step using the Wasserstein distance.

The simple, data-agnostic reference process \mathbb{Q}_t used in previous formulations (De Bie et al., 2019; Chen et al., 2021a) implicitly presumes unrealistic dynamics of \mathbb{P}_t . As a consequence, these models lead to numerical instabilities, high variance in the results, and failure to reconstruct the evolution from $\hat{\mathbb{P}}_0 \rightarrow \hat{\mathbb{P}}_T$ (see Table 2). We remark that, for baselines, the seemingly competitive performance (the 3-4th column in Table 2) comes at the price of extensively tuning the hyperparameters of the reference SDEs (see Appendix D.1). As a result, these baselines are highly inconsistent even though they might perform reasonably well in certain runs. To solidify our point, in the 5-6th column of Table 2, we simply scale the datasets by 20 and observe that the previously high-performing baselines completely fail due to numerical instabilities. In sharp contrast, as our framework is data-adaptive, GSBFLOW consistently succeeds in learning from $\hat{\mathbb{P}}_0$ to $\hat{\mathbb{P}}_T$, outperforming previous methods in all explored settings.

Besides evaluating how well GSBFLOW resembles the spatio-temporal dynamics, we analyze its ability to capture biological heterogeneity. Serving as an *in vitro* model of early embryogenesis, embryoid bodies differentiation captures the development of ESCs into mesoderm, endoderm, neuroectoderm, neural crest and others. Using an initial k -means clustering ($k = 30$) and following Moon et al. (2019, Fig. 6, Suppl. Note 4), we compute lineage branch classes (Fig. 9c) for all cells in a 10-dimensional embedding space using PHATE, a non-linear dimensionality reduction method capturing a denoised representation of both local and global structure of a dataset (Fig. 9b). For details, see Appendix C.2.

We then train a k -NN classifier ($k = 5$) to infer the lineage branch class based on a 30-dimensional PCA embedding of a cell (ESC: 0, neural crest: 1, neuroectoderm: 2, endoderm: 3, mesoderm: 4, other: 5). We analyze the captured lineage branch heterogeneity of GSBFLOW’s predictions by computing the lineage branch class of each cell using the k -NN classifier. The predicted populations colored by the estimated lineage branch as well as the data with the true lineage branch labels are visualized in Fig. 4. We study a more fine-grained resolution of lineage branches into subbranches in Appendix B (Fig. 6). This analysis further demonstrates GSBFLOW’s ability to learn cells’ differentiation into various lineages and to capture biological heterogeneity on a more macroscopic level.

6. Conclusion

Schrödinger bridges promise to provide a powerful tool to infer a wide variety of paths linking particles between two marginals. Estimating such bridges requires determining a backward and forward drift for a pair of coupled SDEs that progressively transform one measure into the other, and vice-versa. This estimation is, however, notoriously difficult: while it is relatively easy to select priors for such drifts that might turn a complex measure onto a simple one (e.g., Gaussian), determining suitable priors for connecting two arbitrarily complex measures is much more challenging. Our proposal fills that gap: we first derive a *closed-form* solution for the Schrödinger bridge between two Gaussians (GSB). We then use these closed-forms on the Gaussian approximation of the marginals, which provides the prior knowledge necessary to estimate the original Schrödinger bridge between the target measures. Our experiments show that this approach performs significantly better than all existing alternatives. A certain limitation of our framework lies in the assumption that the first and second order moments of the marginals are informative. Moreover, in high-dimensions estimating them may be challenging on its own. Our experiments on single-cell data are, however, encouraging, since they show the value of these Gaussian approximations even for moderately high dimensions.

Acknowledgments

This research was supported by the European Research Council (ERC) under the European Union’s Horizon 2020 research and innovation program grant agreement no. 815943 and created as part of NCCR Catalysis (grant number 180544), a National Centre of Competence in Research funded by the Swiss National Science Foundation. Ya-Ping Hsieh acknowledges funding through an ETH Foundations of Data Science (ETH-FDS) postdoctoral fellowship.

References

- D. Alvarez-Melis, Y. Schiff, and Y. Mroueh. Optimizing Functionals on the Space of Probabilities with Input Convex Neural Networks. *arXiv Preprint*, 2021.
- E. Bernton, J. Heng, A. Doucet, and P. E. Jacob. Schrödinger Bridge Samplers. In *arXiv Preprint*, 2019.
- R. Bojilov and A. Galichon. Matching in Closed-Form: Equilibrium, Identification, and Comparative Statics. *Economic Theory*, 61(4), 2016.
- C. Bunne, L. Meng-Papaxanthos, A. Krause, and M. Cuturi. Proximal Optimal Transport Modeling of Population Dynamics. In *International Conference on Artificial Intelligence and Statistics (AISTATS)*, volume 25, 2022.
- T. Chen, G.-H. Liu, and E. A. Theodorou. Likelihood Training of Schrödinger Bridge using Forward-Backward SDEs Theory. In *arXiv Preprint*, 2021a.
- Y. Chen, T. T. Georgiou, and M. Pavon. Optimal steering of a linear stochastic system to a final probability distribution, part I. *IEEE Transactions on Automatic Control*, 61(5), 2015.
- Y. Chen, T. T. Georgiou, and M. Pavon. On the relation between optimal transport and Schrödinger bridges: A stochastic control viewpoint. *Journal of Optimization Theory and Applications*, 169(2), 2016.
- Y. Chen, T. T. Georgiou, and M. Pavon. Stochastic control liaisons: Richard Sinkhorn meets Gaspard Monge on a Schrödinger bridge. *SIAM Review*, 63(2), 2021b.
- M. Cuturi. Sinkhorn Distances: Lightspeed Computation of Optimal Transport. In *Advances in Neural Information Processing Systems (NeurIPS)*, volume 26, 2013.
- G. De Bie, G. Peyré, and M. Cuturi. Stochastic Deep Networks. In *International Conference on Machine Learning (ICML)*, volume 36, 2019.
- V. De Bortoli, A. Doucet, J. Heng, and J. Thornton. Simulating Diffusion Bridges with Score Matching. In *arXiv Preprint*, 2021a.
- V. De Bortoli, J. Thornton, J. Heng, and A. Doucet. Diffusion Schrödinger bridge with applications to score-based generative modeling. In *Advances in Neural Information Processing Systems (NeurIPS)*, volume 35, 2021b.
- E. del Barrio and J.-M. Loubes. The statistical effect of entropic regularization in optimal transportation. *arXiv Preprint*, 2020.
- C. J. Frangieh, J. C. Melms, P. I. Thakore, K. R. Geiger-Schuller, P. Ho, A. M. Luoma, B. Cleary, L. Jerby-Arnon, S. Malu, M. S. Cuoco, et al. Multimodal pooled perturbation-seq screens in patient models define mechanisms of cancer immune evasion. *Nature Genetics*, 53(3), 2021.
- J. Ho, A. Jain, and P. Abbeel. Denoising Diffusion Probabilistic Models. In *Advances in Neural Information Processing Systems (NeurIPS)*, 2020.
- C.-W. Huang, R. T. Q. Chen, C. Tsirigotis, and A. Courville. Convex Potential Flows: Universal Probability Distributions with Optimal Transport and Convex Optimization. In *International Conference on Learning Representations (ICLR)*, 2021a.
- C.-W. Huang, J. H. Lim, and A. Courville. A Variational Perspective on Diffusion-Based Generative Models and Score Matching. In *Advances in Neural Information Processing Systems (NeurIPS)*, 2021b.
- J. Huang, Y. Jiao, L. Kang, X. Liao, J. Liu, and Y. Liu. Schrödinger-Föllmer Sampler: Sampling without Ergodicity. *arXiv Preprint*, 2021c.
- H. Janati, B. Muzellec, G. Peyré, and M. Cuturi. Entropic Optimal Transport between Unbalanced Gaussian Measures has a Closed Form. In *Advances in Neural Information Processing Systems (NeurIPS)*, volume 33, 2020.
- D. P. Kingma and J. Ba. Adam: A Method for Stochastic Optimization. In *International Conference on Learning Representations (ICLR)*, 2014.
- A. Kulkarni, A. G. Anderson, D. P. Merullo, and G. Konopka. Beyond bulk: a review of single cell transcriptomics methodologies and applications. *Current opinion in biotechnology*, 58:129–136, 2019.
- H. Lavenant, S. Zhang, Y.-H. Kim, and G. Schiebinger. Towards a mathematical theory of trajectory inference. *arXiv Preprint*, 2021.
- C. Léonard. A survey of the Schrödinger problem and some of its connections with optimal transport. *arXiv preprint arXiv:1308.0215*, 2013.
- P. Liberali, B. Snijder, and L. Pelkmans. A Hierarchical Map of Regulatory Genetic Interactions in Membrane Trafficking. *Cell*, 157(6), 2014.

- M. D. Luecken and F. J. Theis. Current best practices in single-cell RNA-seq analysis: a tutorial. *Molecular Systems Biology*, 15(6), 2019.
- E. Z. Macosko, A. Basu, R. Satija, J. Nemeshegyi, K. Shekhar, M. Goldman, I. Tirosh, A. R. Bialas, N. Kamitaki, E. M. Martersteck, et al. Highly parallel genome-wide expression profiling of individual cells using nanoliter droplets. *Cell*, 161(5):1202–1214, 2015.
- A. Mallasto, A. Gerolin, and H. Q. Minh. Entropy-regularized 2-Wasserstein distance between Gaussian measures. *Information Geometry*, pages 1–35, 2021.
- R. Mansuy and M. Yor. *Aspects of Brownian motion*. Springer Science & Business Media, 2008.
- G. R. Martin and M. J. Evans. Differentiation of Clonal Lines of Teratocarcinoma Cells: Formation of Embryoid Bodies In Vitro. *Proceedings of the National Academy of Sciences*, 72(4), 1975.
- P. Mokrov, A. Korotin, L. Li, A. Genevay, J. Solomon, and E. Burnaev. Large-Scale Wasserstein Gradient Flows. In *Advances in Neural Information Processing Systems (NeurIPS)*, 2021.
- K. R. Moon, D. van Dijk, Z. Wang, S. Gigante, D. B. Burkhardt, W. S. Chen, K. Yim, A. van den Elzen, M. J. Hirn, R. R. Coifman, et al. Visualizing structure and transitions in high-dimensional biological data. *Nature Biotechnology*, 37(12), 2019.
- M. Pavon, G. Trigila, and E. G. Tabak. The data-driven Schrödinger bridge. *Communications on Pure and Applied Mathematics*, 74(7), 2021.
- G. Peyré and M. Cuturi. Computational Optimal Transport. *Foundations and Trends in Machine Learning*, 11(5-6), 2019. ISSN 1935-8245.
- E. Platen and N. Bruti-Liberati. *Numerical Solution of Stochastic Differential Equations with Jumps in Finance*, volume 64. Springer Science & Business Media, 2010.
- P. E. Protter. Stochastic differential equations. In *Stochastic Integration and Differential Equations*, pages 249–361. Springer, 2005.
- D. Rezende and S. Mohamed. Variational Inference with Normalizing Flows. In *International Conference on Machine Learning (ICML)*, 2015.
- G. Schiebinger, J. Shu, M. Tabaka, B. Cleary, V. Subramanian, A. Solomon, J. Gould, S. Liu, S. Lin, P. Berube, et al. Optimal-Transport Analysis of Single-Cell Gene Expression Identifies Developmental Trajectories in Reprogramming. *Cell*, 176(4), 2019.
- E. Schrödinger. *Über die Umkehrung der Naturgesetze*. Verlag der Akademie der Wissenschaften in Kommission bei Walter De Gruyter u. Company, 1931.
- E. Schrödinger. Sur la théorie relativiste de l'électron et l'interprétation de la mécanique quantique. In *Annales de l'institut Henri Poincaré*, volume 2, 1932.
- M. J. Shablott, C. L. Kerr, J. Axelman, J. W. Littlefield, G. O. Clark, E. S. Patterson, R. C. Addis, J. N. Kraszewski, K. C. Kent, and J. D. Gearhart. Derivation and Differentiation of Human Embryonic Germ Cells. In *Essentials of Stem Cell Biology*. Elsevier, 2009.
- J. Sohl-Dickstein, E. Weiss, N. Maheswaranathan, and S. Ganguli. Deep Unsupervised Learning using Nonequilibrium Thermodynamics. In *International Conference on Machine Learning (ICML)*, 2015.
- Y. Song and S. Ermon. Generative Modeling by Estimating Gradients of the Data Distribution. In *arXiv Preprint*, 2019.
- Y. Song, J. Sohl-Dickstein, D. P. Kingma, A. Kumar, S. Ermon, and B. Poole. Score-Based Generative Modeling through Stochastic Differential Equations. In *International Conference on Learning Representations (ICLR)*, volume 9, 2021.
- A. Tong, J. Huang, G. Wolf, D. Van Dijk, and S. Krishnaswamy. TrajectoryNet: A Dynamic Optimal Transport Network for Modeling Cellular Dynamics. In *International Conference on Machine Learning (ICML)*, 2020.
- user26872. Reference for Multidimensional Gaussian Integral. Mathematics Stack Exchange. URL <https://math.stackexchange.com/q/126767>. URL: <https://math.stackexchange.com/q/126767> (version: 2012-04-01).
- F. Vargas, P. Thodoroff, N. D. Lawrence, and A. Lamacraft. Solving Schrödinger Bridges via Maximum Likelihood. *arXiv Preprint*, 2021.
- G. Wang, Y. Jiao, Q. Xu, Y. Wang, and C. Yang. Deep Generative Learning via Schrödinger Bridge. In *International Conference on Machine Learning (ICML)*, 2021.
- F. A. Wolf, P. Angerer, and F. J. Theis. SCANPY: large-scale single-cell gene expression data analysis. *Genome Biology*, 19(1), 2018.
- A. Zee. *Quantum Field Theory in a Nutshell*, volume 7. Princeton University Press, 2010.
- G. X. Zheng, J. M. Terry, P. Belgrader, P. Ryvkin, Z. W. Bent, R. Wilson, S. B. Zivaldo, T. D. Wheeler, G. P. McDermott, J. Zhu, et al. Massively parallel digital transcriptional profiling of single cells. *Nature Communications*, 8(1), 2017.

A. Proof of the Closed-Form Solutions for Gaussian Schrödinger Bridges

A.1. Preliminaries for the Proof of Theorem 1

Let $\xi \sim \mathcal{N}(\mu, \Sigma)$ and $\xi' \sim \mathcal{N}(\mu', \Sigma')$. The *static* Gaussian SB problem, alternatively known as entropic optimal transport (Peyré and Cuturi, 2019), is defined as

$$\min_{\pi \in \Pi(\xi, \xi')} \int_{\mathbb{R}^d \times d} \frac{\|x - x'\|_2^2}{2} d\pi(x, x') + \sigma^2 D_{\text{KL}}(\pi \| \xi \otimes \xi') \quad (\text{Static-GSB})$$

where $\Pi(\xi, \xi')$ denotes the set of all coupling between ξ and ξ' . We will need the solution of (Static-GSB) in the following form (Janati et al., 2020, Theorem 1):

Lemma A.1 (Exact solutions of (Static-GSB)). *The solution to (Static-GSB) is given by*

$$\pi^* \sim \mathcal{N}\left(\begin{bmatrix} \mu \\ \mu' \end{bmatrix}, \begin{bmatrix} \Sigma & C_\sigma \\ C_\sigma^\top & \Sigma' \end{bmatrix}\right) \quad (\text{A.1})$$

where C_σ is defined in Section 3.2 with $\Sigma_0 \leftarrow \Sigma$ and $\Sigma_T \leftarrow \Sigma'$.

We also need a technical lemma that is intimately related to the ‘‘central identity of quantum field theory’’ (Zee, 2010); the version below is adopted from (user26872), wherein the readers can find an easy proof.

Lemma A.2 (The central identity of Quantum Field Theory). *The following identity holds for all matrix $M \succ 0$ and all sufficiently regular analytic function v (e.g., polynomials or $v \in C^\infty(\mathbb{R}^d)$ with compact support):*

$$(2\pi)^{-\frac{d}{2}} (\det M)^{-\frac{1}{2}} \int_{\mathbb{R}^d} v(x) \exp\left(-\frac{1}{2} x^\top M x\right) dx = \exp\left(\frac{1}{2} \partial_x^\top M^{-1} \partial_x\right) v(x) \Big|_{x=0} \quad (\text{A.2})$$

where $\exp\left(\frac{1}{2} \partial_x^\top M^{-1} \partial_x\right)$ is understood as a power series in the differential operators.

Lastly, we recall the elementary

Lemma A.3 (Conditional Gaussians are Gaussian). *Let $(Y_0, Y_1) \sim \mathcal{N}\left(\begin{bmatrix} \mu_0 \\ \mu_1 \end{bmatrix}, \begin{bmatrix} \Sigma_{00} & \Sigma_{01} \\ \Sigma_{10} & \Sigma_{11} \end{bmatrix}\right)$. Then $Y_0 | Y_1 = y \sim \mathcal{N}(\check{\mu}, \check{\Sigma})$*

where

$$\begin{aligned} \check{\mu} &= \mu_0 + \Sigma_{01} \Sigma_{11}^{-1} (y - \mu_1), \\ \check{\Sigma} &= \Sigma_{00} - \Sigma_{01} \Sigma_{11}^{-1} \Sigma_{10}. \end{aligned} \quad (\text{A.3})$$

A.2. The Proof

We are now ready for the proof. For convenience, we restate Theorem 1 below:

Theorem 1. *Denote by \mathbb{P}_t^* the solution to (SB \mathcal{N}). Set*

$$\begin{aligned} r_t &:= \frac{\kappa(t, T)}{\kappa(T, T)}, \quad \bar{r}_t := \tau_t - r_t \tau_T, \quad \sigma_* := \sqrt{\tau_T^{-1} \kappa(T, T)}, \\ \zeta(t) &:= \tau_t \int_0^t \tau_s^{-1} \alpha(s) ds, \quad \rho_t := \frac{\int_0^t \tau_s^{-2} g^2(s) ds}{\int_0^T \tau_s^{-2} g^2(s) ds}, \\ P_t &:= \dot{r}_t (r_t \Sigma_T + \bar{r}_t C_{\sigma_*}), \quad Q_t := -\dot{\bar{r}}_t (\bar{r}_t \Sigma_0 + r_t C_{\sigma_*}), \\ S_t &:= P_t - Q_t^\top + [c(t) \kappa(t, t) (1 - \rho_t) - g^2(t) \rho_t] I. \end{aligned} \quad (9)$$

Then the following holds:

1. *The solution \mathbb{P}_t^* is a Markov Gaussian process whose marginal variable X_t^* follows $\mathcal{N}(\mu_t^*, \Sigma_t^*)$, where*

$$\mu_t^* := \bar{r}_t \mu_0 + r_t \mu_T + \zeta(t) - r_t \zeta(T), \quad (10)$$

$$\begin{aligned} \Sigma_t^* &:= \bar{r}_t^2 \Sigma_0 + r_t^2 \Sigma_T + r_t \bar{r}_t (C_{\sigma_*} + C_{\sigma_*}^\top) \\ &\quad + \kappa(t, t) (1 - \rho_t) I. \end{aligned} \quad (11)$$

2. *X_t^* admits a closed-form solution as the SDE:*

$$dX_t^* = f_{\mathcal{N}}(t, X_t^*) dt + g(t) d\mathbb{W}_t \quad (12)$$

where

$$f_{\mathcal{N}}(t, x) := S_t^\top \Sigma_t^{*-1} (x - \mu_t^*) + \dot{\mu}_t^*. \quad (13)$$

Moreover, the matrix $S_t^\top \Sigma_t^{*-1}$ is symmetric.

Proof of Theorem 1. From now on, we will invoke the notations in (9) without explicit mentions.

The static Gaussian SB. We begin by solving the *static* Gaussian SB

$$\min_{\mathbb{P}_{0T}} D_{\text{KL}}(\mathbb{P}_{0T} \| \mathbb{Q}_{0T}) \quad (\text{A.4})$$

over all \mathbb{P}_{0T} having marginals $\mathcal{N}(\mu_0, \Sigma_0)$ and $\mathcal{N}(\mu_T, \Sigma_T)$.

Recall that, conditioned on Y_0 , $Y_t \sim \mathbb{Q}_t$ is a Gaussian process with mean (7) and covariance (8). Thus, if we only consider the endpoint marginal distributions (Y_0, Y_T) , it is easy to derive the transition probability:

$$\mathbb{Q}(Y_T = y_T | Y_0 = y_0) = (2\pi)^{\frac{d}{2}} \det(\kappa(T, T)I)^{-\frac{1}{2}} \exp\left(-\frac{1}{2}(y_T - \eta(T))^\top (\kappa(T, T)I)^{-1} (y_T - \eta(T))\right) \quad (\text{A.5})$$

$$= (2\pi)^{\frac{d}{2}} \det(\kappa(T, T)I)^{-\frac{1}{2}} \exp\left(-\frac{1}{2\kappa(T, T)} \|y_T - \tau_T y_0 - \zeta(T)\|^2\right). \quad (\text{A.6})$$

Therefore, abusing the notation by continually writing \mathbb{P}_{0T} as the relative density of \mathbb{P}_{0T} with respect to the Lebesgue measure, we get

$$D_{\text{KL}}(\mathbb{P}_{0T} \| \mathbb{Q}_{0T}) = \int_{\mathbb{R}^d \times \mathbb{R}^d} \log \frac{d\mathbb{P}_{0T}}{d\mathbb{Q}_{0T}} d\mathbb{P}_{0T} \quad (\text{A.7})$$

$$= \text{const.} + \frac{1}{2\kappa(T, T)} \int_{\mathbb{R}^d \times \mathbb{R}^d} \|y' - \tau_T y - \tau_T \zeta(T)\|^2 d\mathbb{P}_{0T}(y, y') + \int_{\mathbb{R}^d \times \mathbb{R}^d} \log \mathbb{P}_{0T} d\mathbb{P}_{0T}. \quad (\text{A.8})$$

If \mathbb{P}_{0T} is a joint distribution with marginals $Y \sim \mathcal{N}(\mu_0, \Sigma_0)$ and $Y' \sim \mathcal{N}(\mu_T, \Sigma_T)$, then the change of variable $\tilde{Y} = \tau_T Y + \zeta(T)$ gives rise to a joint distribution $\tilde{\mathbb{P}}_{0T}$ having marginals $\tilde{Y} \sim \mathcal{N}(\tilde{\mu}_0, \tilde{\Sigma}_0)$ and $Y' \sim \mathcal{N}(\mu_T, \Sigma_T)$, where

$$\tilde{\mu}_0 = \tau_T \mu_0 + \zeta(T), \quad (\text{A.9})$$

$$\tilde{\Sigma}_0 = \tau_T^2 \Sigma_0. \quad (\text{A.10})$$

Obviously, there is a one-to-one correspondence between \mathbb{P}_{0T} and $\tilde{\mathbb{P}}_{0T}$.

The first integral in (A.8) is equal to $\mathbb{E} \left[\|Y' - \tilde{Y}\|^2 \right]$. On the other hand, we always have

$$\int_{\mathbb{R}^d \times \mathbb{R}^d} \log \tilde{\mathbb{P}}_{0T} d\tilde{\mathbb{P}}_{0T} = \int_{\mathbb{R}^d \times \mathbb{R}^d} \log \mathbb{P}_{0T} d\mathbb{P}_{0T} + \text{const.}$$

Therefore, minimizing (A.7) over \mathbb{P}_{0T} is equivalent to

$$\min_{\tilde{\mathbb{P}}_{0T}} D_{\text{KL}}(\tilde{\mathbb{P}}_{0T} \| \mathbb{Q}_{0T}) \equiv \min_{\tilde{\mathbb{P}}_{0T}} \int_{\mathbb{R}^d \times \mathbb{R}^d} \frac{\|y - y'\|_2^2}{2} d\tilde{\mathbb{P}}_{0T}(y, y') + \kappa(T, T) \int_{\mathbb{R}^d \times \mathbb{R}^d} \log \tilde{\mathbb{P}}_{0T} d\tilde{\mathbb{P}}_{0T}. \quad (\text{A.11})$$

By Lemma A.1, the solution to (A.11) is given by the joint Gaussian

$$\tilde{\mathbb{P}}_{0T}^* \sim \mathcal{N}\left(\begin{bmatrix} \tilde{\mu}_0 \\ \mu_T \end{bmatrix}, \begin{bmatrix} \tilde{\Sigma}_0 & \tilde{C}_{\tilde{\sigma}} \\ \tilde{C}_{\tilde{\sigma}}^\top & \Sigma_T \end{bmatrix}\right) \quad (\text{A.12})$$

where $\tilde{\sigma} = \sqrt{\kappa(T, T)}$ and

$$\tilde{C}_{\tilde{\sigma}} = \frac{1}{2} \left(\tilde{\Sigma}_0^{\frac{1}{2}} \tilde{D}_{\tilde{\sigma}} \tilde{\Sigma}_0^{-\frac{1}{2}} - \tilde{\sigma}^2 I \right), \quad (\text{A.13})$$

$$\tilde{D}_{\tilde{\sigma}} = \left(4 \tilde{\Sigma}_0^{\frac{1}{2}} \Sigma_T \tilde{\Sigma}_0^{\frac{1}{2}} + \tilde{\sigma}^4 I \right)^{\frac{1}{2}}. \quad (\text{A.14})$$

The optimal static Gaussian SB \mathbb{P}_{0T}^* is then given by the inverse transform $Y = \tau_T^{-1}(\tilde{Y} - \zeta(T))$, i.e.,

$$\mathbb{P}_{0T}^* \sim \mathcal{N} \left(\begin{bmatrix} \mu_0 \\ \mu_T \end{bmatrix}, \begin{bmatrix} \Sigma_0 & \tau_T^{-1} \tilde{C}_{\tilde{\sigma}} \\ \tau_T^{-1} \tilde{C}_{\tilde{\sigma}}^\top & \Sigma_T \end{bmatrix} \right). \quad (\text{A.15})$$

Rearranging terms and using (A.13) and (A.14), we get

$$\tau_T^{-1} \tilde{C}_{\tilde{\sigma}} = C_{\sigma_*} \quad (\text{A.16})$$

where $\sigma_* = \frac{\kappa(T, T)}{\tau_T}$.

The \mathbb{Q} -Bridges. For future use, we will need the distribution of Y_t conditioned on Y_0 and Y_T . When $Y_t \equiv \mathbb{W}_t$, the distribution is called the *Brownian bridge*, which is in itself an important subject in mathematics and financial engineering (Mansuy and Yor, 2008). We thus term the conditional distribution of Y_t the \mathbb{Q} -Bridges.

From (7) and (8), one can infer that, given Y_0 , the joint distribution of (Y_t, Y_T) is

$$Y_t, Y_T | Y_0 \sim \mathcal{N} \left(\begin{bmatrix} \eta(t) \\ \eta(T) \end{bmatrix}, \begin{bmatrix} \kappa(t, t) I & \kappa(t, T) I \\ \kappa(t, T) I & \kappa(T, T) I \end{bmatrix} \right). \quad (\text{A.17})$$

Therefore, Lemma A.3 applied implies that, conditioned on Y_0 and Y_T , Y_t is Gaussian with mean

$$\begin{aligned} \mathbb{E}[Y_t | Y_0, Y_T] &= \eta(t) + \frac{\kappa(t, T)}{\kappa(T, T)} (Y_T - \eta(T)) \\ &= \tau_t Y_0 + \zeta(t) + \frac{\kappa(t, T)}{\kappa(T, T)} (Y_T - \tau_T Y_0 - \zeta(T)) \\ &= \left(\tau_t - \frac{\kappa(t, T)}{\kappa(T, T)} \tau_T \right) Y_0 + \frac{\kappa(t, T)}{\kappa(T, T)} Y_T + \zeta(t) - \frac{\kappa(t, T)}{\kappa(T, T)} \zeta(T) \\ &= \bar{r}_t Y_0 + r_t Y_T + \zeta(t) - \tau_t \zeta(T) \end{aligned} \quad (\text{A.18})$$

and covariance process (for any $t' \geq t$)

$$\mathbb{E} \left[(Y_t - \mathbb{E}[Y_t | Y_0, Y_T]) (Y_{t'} - \mathbb{E}[Y_{t'} | Y_0, Y_T])^\top \mid Y_0, Y_T \right] = \left(\kappa(t, t') - \frac{\kappa(t, T) \kappa(t', T)}{\kappa(T, T)} \right) I. \quad (\text{A.19})$$

Since a Gaussian process is uniquely determined by its mean and covariance processes, we have, for some Gaussian process ξ_t independent of Y_t having zero mean and covariance process (A.19),

$$Y_t | Y_0, Y_T \stackrel{\text{law}}{=} \bar{r}_t Y_0 + r_t Y_T + \zeta(t) - \tau_t \zeta(T) + \xi_t. \quad (\text{A.20})$$

From \mathbb{Q} -Bridges to μ_t^* and Σ_t^* . The disintegration formula of $D_{\text{KL}}(\cdot \| \cdot)$ (Léonard, 2013) implies that the solution to (SB $_{\mathcal{N}}$) is given by first generating $(X_0^*, X_T^*) \sim \mathbb{P}_{0T}^*$ for \mathbb{P}_{0T}^* in (A.15), and then connecting X_0^* and X_T^* using the \mathbb{Q} -bridges (A.20). Namely,

$$X_t^* \stackrel{\text{law}}{=} \bar{r}_t X_0^* + r_t X_T^* + \zeta(t) - \tau_t \zeta(T) + \xi_t \quad (\text{A.21})$$

from which (10) and (11) follow by a straightforward calculation. Furthermore, in view of (A.15) and (A.21), X_t^* is obviously a Gaussian process. Finally, since \mathbb{Q}_t is a Markov process, (Léonard, 2013, Theorem 2.12) implies that \mathbb{P}_t^* is also Markov. This concludes the first half of Theorem 1.

The SDE representation of X_t^* . The main idea of proving (13) is to compute

$$\lim_{h \rightarrow 0} \frac{\mathbb{E}[u(t+h, X_{t+h}^*) \mid X_t^* = x] - u(t, x)}{h} \quad (\text{A.22})$$

and equate (A.22) with the *generator* of (12), which is (Protter, 2005)

$$\mathcal{L}_t u(t, x) := \frac{\partial}{\partial t} u(t, x) + \frac{g^2(t)}{2} \Delta u(t, x) + \langle \nabla u(t, x), f_{\mathcal{N}}(t, x) \rangle. \quad (\text{A.23})$$

Since X_t^* is a Gaussian process, we may derive the conditional expectation in (A.22) using Lemma A.3. However, since eventually we will divide everything by h and drive $h \rightarrow 0$, we can ignore any term that is $o(h)$ during the computation. This simple observation will prove to be extremely useful in the sequel.

We first compute the first-order approximation of Σ_t^* . In view of (11), and since $r_t \kappa(t, T) = \kappa(t, t) \rho_t$ and $\dot{r}_t \kappa(t, T) = r_t \frac{\partial}{\partial t} \kappa(t, T)$, we have

$$\begin{aligned} \dot{\Sigma}_t^* &= 2\dot{\bar{r}}_t \bar{r}_t \Sigma_0 + 2\dot{r}_t r_t \Sigma_T + (\dot{r}_t \bar{r}_t + r_t \dot{\bar{r}}_t) (C_{\sigma_*} + C_{\sigma_*}^\top) + \left(\frac{\partial}{\partial t} \kappa(t, t) - \dot{r}_t \kappa(t, T) - r_t \frac{\partial}{\partial t} \kappa(t, T) \right) I \\ &= \dot{r}_t (r_t \Sigma_T + \bar{r}_t C_{\sigma_*} + r_t \Sigma_T + \bar{r}_t C_{\sigma_*}^\top) + \dot{\bar{r}}_t (\bar{r}_t \Sigma_0 + r_t C_{\sigma_*} + \bar{r}_t \Sigma_0 + r_t C_{\sigma_*}^\top) + \left(\frac{\partial}{\partial t} \kappa(t, t) - 2\dot{r}_t \kappa(t, T) \right) I \\ &= (P_t + P_t^\top) - (Q_t + Q_t^\top) + \left(\frac{\partial}{\partial t} \kappa(t, t) - 2\dot{r}_t \kappa(t, T) \right) I. \end{aligned} \quad (\text{A.24})$$

Next, let $K_{t, t+h}$ denote the covariance process of X_t^* . We can estimate $K_{t, t+h}$ up to first order by computing:

$$\begin{aligned} K_{t, t+h} &:= \mathbb{E} \left[(X_t^* - \mu_t^*) (X_{t+h}^* - \mu_{t+h}^*)^\top \right] \\ &= \bar{r}_t \bar{r}_{t+h} \Sigma_0 + r_t r_{t+h} \Sigma_T + \bar{r}_t r_{t+h} C_{\sigma_*} + r_t \bar{r}_{t+h} C_{\sigma_*}^\top + (\kappa(t, t+h) - r_{t+h} \kappa(t, T)) I \\ &= \Sigma_t^* + \bar{r}_t (\bar{r}_{t+h} - \bar{r}_t) \Sigma_0 + r_t (r_{t+h} - r_t) \Sigma_T + \bar{r}_t (r_{t+h} - r_t) C_{\sigma_*} + r_t (\bar{r}_{t+h} - \bar{r}_t) C_{\sigma_*}^\top \\ &\quad + (\kappa(t, t+h) - \kappa(t, t) - r_{t+h} \kappa(t, T) + r_t \kappa(t, T)) I \\ &= \Sigma_t^* + \frac{r_{t+h} - r_t}{\dot{r}_t} P_t - \frac{\bar{r}_{t+h} - \bar{r}_t}{\dot{\bar{r}}_t} Q_t^\top + (\kappa(t, t+h) - \kappa(t, t) - r_{t+h} \kappa(t, T) + r_t \kappa(t, T)) I \\ &= \Sigma_t^* + h \left\{ P_t - Q_t^\top + \left[\left(\frac{\partial}{\partial t'} \kappa \right) (t, t) - \dot{r}_t \kappa(t, T) \right] I \right\} + o(h) \end{aligned} \quad (\text{A.25})$$

where $\left(\frac{\partial}{\partial t'} \kappa \right) (t, t') := \lim_{h \rightarrow 0} \frac{\kappa(t, t'+h) - \kappa(t, t')}{h}$ denotes the derivative of the function $\kappa(t, \cdot)$. Using (8) and $\dot{r}_t = c(t) \tau_t$, we have

$$\left(\frac{\partial}{\partial t'} \kappa \right) (t, t) = \frac{\partial}{\partial t'} \left(\tau_t \tau_{t'} \int_0^t \tau_s^{-2} g^2(s) ds \right) \Big|_{t'=t} \quad (\text{A.26})$$

$$\begin{aligned} &= \dot{r}_t \tau_t \int_0^t \tau_s^{-2} g^2(s) ds \\ &= c(t) \kappa(t, t). \end{aligned} \quad (\text{A.27})$$

On the other hand, we have

$$\begin{aligned} \dot{r}_t &= \frac{1}{\kappa(T, T)} \frac{\partial}{\partial t} \left(\tau_t \tau_T \int_0^t \tau_s^{-2} g^2(s) ds \right) \\ &= \frac{1}{\kappa(T, T)} (c(t) \kappa(t, T) + \tau_t^{-1} \tau_T g^2(t)) \\ &= c(t) r_t + \frac{\tau_T g^2(t)}{\tau_t \kappa(T, T)}. \end{aligned} \quad (\text{A.28})$$

Combining (A.27) and (A.28), using the fact that $r_t \kappa(t, T) = \kappa(t, t) \rho_t$ and $\frac{\tau_T \kappa(t, T)}{\tau_t \kappa(T, T)} = \rho_t$, we may further write (A.25) as

$$\begin{aligned} K_{t, t+h} &= \Sigma_t^* + h \{ P_t - Q_t^\top + [c(t) \kappa(t, t) (1 - \rho_t) - g^2(t) \rho_t] I \} + o(h) \\ &= \Sigma_t^* + h S_t + o(h). \end{aligned} \quad (\text{A.29})$$

We are now ready to derive (12). By Lemma A.3, the random variable X_{t+h}^* conditioned on $X_t^* = x$ follows $\mathcal{N}(\check{\mu}_{t+h}, \check{\Sigma}_{t+h})$

where, by (A.29),

$$\begin{aligned}
 \check{\mu}_{t+h} &= \mu_{t+h}^* + K_{t,t+h}^\top \Sigma_t^{*-1} (x - \mu_t^*) \\
 &= \mu_t^* + h\dot{\mu}_t^* + (I + hS_t^\top \Sigma_t^{*-1})(x - \mu_t^*) + o(h) \\
 &= x + h(S_t^\top \Sigma_t^{*-1}(x - \mu_t^*) + \dot{\mu}_t^*) + o(h),
 \end{aligned} \tag{A.30}$$

and, by (A.24) and (A.25),

$$\begin{aligned}
 \check{\Sigma}_{t+h} &= \Sigma_{t+h}^* - K_{t,t+h}^\top \Sigma_t^{*-1} K_{t,t+h} \\
 &= \Sigma_t^* + h\dot{\Sigma}_t^* - (\Sigma_t^* + hS_t^\top + hS_t) + o(h) \\
 &= h \left[P_t + P_t^\top - Q_t - Q_t^\top + \left(\frac{\partial}{\partial t} \kappa(t, t) - 2\dot{r}_t \kappa(t, T) \right) I \right. \\
 &\quad \left. - \left(P_t - Q_t^\top + \left[\left(\frac{\partial}{\partial t'} \kappa \right) (t, t) - \dot{r}_t \kappa(t, T) \right] I \right)^\top - \left(P_t - Q_t^\top + \left[\left(\frac{\partial}{\partial t'} \kappa \right) (t, t) - \dot{r}_t \kappa(t, T) \right] I \right) \right] + o(h) \\
 &= h \left(\frac{\partial}{\partial t} \kappa(t, t) - 2 \left(\frac{\partial}{\partial t'} \kappa \right) (t, t) \right) I + o(h).
 \end{aligned} \tag{A.31}$$

However, by (8), we have

$$\begin{aligned}
 \frac{\partial}{\partial t} \kappa(t, t) &= \frac{\partial}{\partial t} \left(\tau_t^2 \int_0^t \tau_s^{-2} g^2(s) ds \right) \\
 &= 2\dot{r}_t \tau_t \int_0^t \tau_s^{-2} g^2(s) ds + g^2(t), \\
 \left(\frac{\partial}{\partial t'} \kappa \right) (t, t) &= \frac{\partial}{\partial t'} \left(\tau_t \tau_{t'} \int_0^t \tau_s^{-2} g^2(s) ds \right) \Big|_{t'=t}
 \end{aligned} \tag{A.32}$$

$$= \dot{r}_t \tau_t \int_0^t \tau_s^{-2} g^2(s) ds, \tag{A.33}$$

from which (A.31) simplifies to

$$\check{\Sigma}_{t+h} = hg^2(t)I + o(h). \tag{A.34}$$

We can now compute $\mathbb{E}[u(t+h, X_{t+h}^*) | X_t^* = x]$ as follows:

$$\begin{aligned}
 \mathbb{E}[u(t+h, X_{t+h}^*) | X_t^* = x] &= (2\pi)^{\frac{d}{2}} (\det \check{\Sigma}_{t+h})^{-\frac{1}{2}} \int_{\mathbb{R}^d} u(t+h, x') \exp\left(-\frac{1}{2}(x' - \check{\mu}_{t+h})^\top \check{\Sigma}_{t+h}^{-1} (x' - \check{\mu}_{t+h})\right) dx' \\
 &= (2\pi)^{\frac{d}{2}} (\det \check{\Sigma}_{t+h})^{-\frac{1}{2}} \int_{\mathbb{R}^d} u(t+h, x' + \check{\mu}_{t+h}) \exp\left(-\frac{1}{2}x'^\top \check{\Sigma}_{t+h}^{-1} x'\right) dx'.
 \end{aligned} \tag{A.35}$$

Invoking Lemma A.2, we see that (A.35) can be evaluated as

$$\mathbb{E}[u(t+h, X_{t+h}^*) | X_t^* = x] = \exp\left(\frac{1}{2} \partial_{x'}^\top \check{\Sigma}_{t+h} \partial_{x'}\right) u(t+h, x' + \check{\mu}_{t+h}) \Big|_{x'=0}. \tag{A.36}$$

Since $\check{\Sigma}_{t+h} = hg^2(t)I + o(h)$ by (A.34), expanding the power series $\exp(\frac{1}{2} \partial_{x'}^\top \check{\Sigma}_{t+h} \partial_{x'})$ and ignoring every $o(h)$ terms, (A.36) becomes

$$\begin{aligned}
 \mathbb{E}[u(t+h, X_{t+h}^*) | X_t^* = x] &= \left(u(t+h, x' + \check{\mu}_{t+h}) + \frac{hg^2(t)}{2} \Delta u(t+h, x' + \check{\mu}_{t+h}) \right) \Big|_{x'=0} + o(h) \\
 &= u(t+h, \check{\mu}_{t+h}) + \frac{hg^2(t)}{2} \Delta u(t+h, \check{\mu}_{t+h}) + o(h).
 \end{aligned} \tag{A.37}$$

Recalling from (A.30) that $\check{\mu}_{t+h} = x + h(S_t^\top \Sigma_t^{*-1}(x - \mu_t^*) + \dot{\mu}_t^*) + o(h)$, the Taylor expansion in the x variable for $u(t, x)$ shows that

$$\mathbb{E}[u(t+h, X_{t+h}^*) \mid X_t^* = x] = u(t+h, x) + h \left(\frac{g^2(t)}{2} \Delta u(t+h, x) + \langle \nabla u(t+h, x), S_t^\top \Sigma_t^{*-1} (x - \mu_t^*) + \dot{\mu}_t^* \rangle \right) + o(h)$$

whence

$$\lim_{h \rightarrow 0} \frac{\mathbb{E}[u(t+h, X_{t+h}^*) \mid X_t^* = x] - u(t, x)}{h} = \frac{\partial}{\partial t} u(t, x) + \frac{g^2(t)}{2} \Delta u(t, x) + \langle \nabla u(t, x), S_t^\top \Sigma_t^{*-1} (x - \mu_t^*) + \dot{\mu}_t^* \rangle.$$

This is exactly (A.23) with $f_{\mathcal{N}}(t, x) \leftarrow S_t^\top \Sigma_t^{*-1} (x - \mu_t^*) + \dot{\mu}_t^*$, which concludes the proof for (12) and (13).

Finally, by (Léonard, 2013, (4.2)), the optimal drift $f_{\mathcal{N}}(t, x)$ is a *gradient field*:

$$f_{\mathcal{N}}(t, x) = \nabla \psi(t, x) \tag{A.38}$$

for some function $\psi : \mathbb{R}^+ \times \mathbb{R}^d \rightarrow \mathbb{R}$, implying that $S_t^\top \Sigma_t^{*-1}$ must be symmetric. \square

B. Further Experimental Results

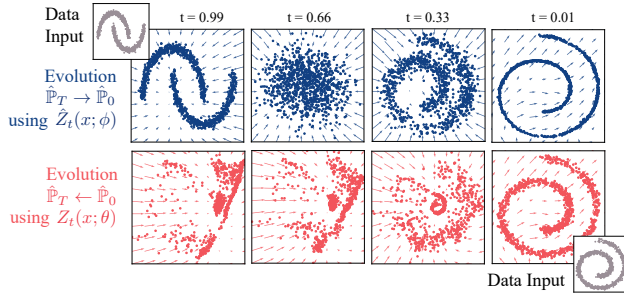
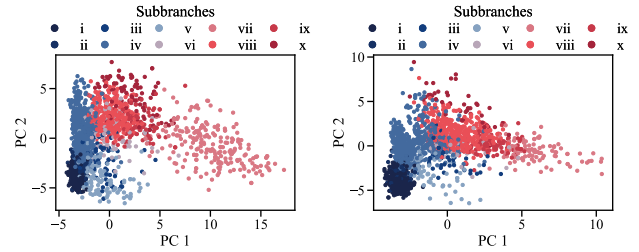


Figure 5. Illustration of the time-dependent drifts learned by (Chen et al., 2021a) with sub-VP SDE for two toy marginal distributions. *Top.* Evolution of $\hat{\mathbb{P}}_T$ (moons) \rightarrow $\hat{\mathbb{P}}_0$ (spiral) via backward policy $\hat{Z}_t^\phi(x)$. *Bottom.* Evolution of $\hat{\mathbb{P}}_0$ (spiral) \rightarrow $\hat{\mathbb{P}}_T$ (moons) via forward policy $\hat{Z}_t^\theta(x)$.



(a) Data

(b) GSBFLOW

Figure 6. PCA embedding of the (a) Moon et al. (2019) data and (b) the GSBFLOW predictions colored by the lineage sub‘branch class.

We present further experimental evidence in this section. Fig. 5 repeats the same synthetic setup for the same baseline (Chen et al., 2021b) as in Section 5, but with the reference process changed sub-VP SDE. The outcome is essentially the same as in the VE SDE case presented in the main text.

Fig. 6 shows the GSBFLOW’s prediction of cell lineages on another dataset (Schiebinger et al., 2019). The result agrees with our observations on the (Moon et al., 2019) dataset present in the main text, where GSBFLOW succeeds in learning the cell’s differentiation into various cell lineages and capturing biological heterogeneity on a more macroscopic level.

C. Single-Cell Datasets

We evaluate GSBFLOW on multiple datasets. This includes synthetic population dynamics, whose results are described in Section 5.1, as well as dynamics of single-cells of a human developmental process, which we cover in Section 5.2. In the following, we describe the data collection and data preprocessing steps.

In biology, developmental processes involve complex tasks such as tissue and organ development, body axis formation, cell division, and cell differentiation, i.e., the development of stem cells into functional cell types. One prototype of such a process is the differentiation of *embryonic stem cells* (ESCs) into distinct lineages such as hematopoietic, cardiac, neural, pancreatic, hepatocytic and germ. It is possible to approximate this development *in vitro* via embryoid bodies (EBs) (Martin and Evans, 1975), three-dimensional aggregates of pluripotent stem cells, including ESCs (Shamblott et al., 2009). Recently, an scRNA-seq analysis is conducted by Moon et al. (2019) in order to unveil the developmental trajectories, as well as cellular and molecular identities through which early lineage precursors emerge from human ESCs. The dataset of (Moon et al., 2019) can be found online via Mendeley Data (V6N743H5NG).

In the second task we consider, the natural developmental process is inverted and instead we study the reprogramming of somatic cells into iPSCs. In a recent study, [Schiebinger et al. \(2019\)](#) unveiled this process in depth by measuring 315,000 single-cell RNA sequencing (scRNA-seq) profiles, collected at half-day intervals across 18 days.

In the following, we provide details for the preprocessing of the raw scRNA-seq data as well as the lineage branch analysis extracting the functional cell types emerging in this developmental process. This dataset can be found via [GEO: GSE122662](#).

C.1. Data Preprocessing

To preprocess the data, we follow the analysis of [Moon et al. \(2019\)](#) as well as [Luecken and Theis \(2019\)](#). For the analysis, we invoke the Python package `scanpy` ([Wolf et al., 2018](#)).

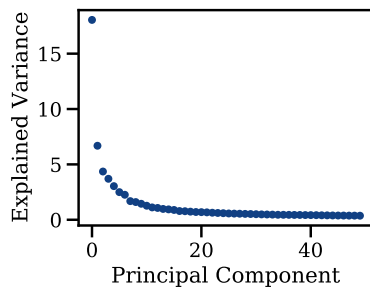


Figure 7. Proportion of explained variance per principal component of the embryoid body scRNA-seq data after preprocessing ([Moon et al., 2019](#)).

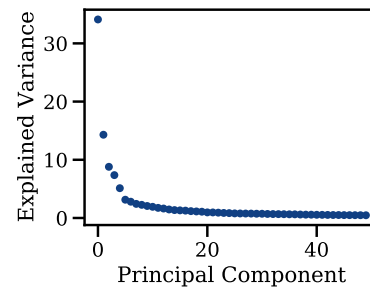


Figure 8. Proportion of explained variance per principal component of MEFs reprogramming into iPSCs after preprocessing ([Schiebinger et al., 2019](#)).

[Moon et al. \(2019\)](#) take measures of approximately 31,000 cells over a 27-day differentiation time course, comprising gene expression matrices and barcodes, i.e., DNA tags for identifying reads originating from the same cell. Subsequently, the measured cells are filtered in a quality control stage, their gene expression levels normalized and further processed in a feature selection step, where only highly-differentiated genes are selected. The resulting data is then visualized using a standard PCA as well as the dimensionality reduction method of PHATE ([Moon et al., 2019](#)) in order to extract biological labels.

The quality control of the data is based on the number of counts per barcode (count depth), the number of genes per barcode, and the fraction of counts from mitochondrial genes per barcode. In our experiments, we only keep cells with at least 4000 and at most 10000 counts, as well as more than 550 expressed genes and less than 20% of mitochondrial counts, as a high fraction is indicative of cells whose cytoplasmic mRNA has leaked out through a broken membrane ([Luecken and Theis, 2019](#)). For the subsequent analysis, we further screen out genes which are expressed in less than 10 genes. After quality control procedure described above, the dataset consists of 15150 cells and 17945 genes. We then normalize each cell by total counts over all genes and logarithmize the data matrix. We extract 4000 highly variable genes (HVG) the 10X genomics preprocessing software `Cell Ranger` ([Zheng et al., 2017](#)) to further reduce the dimensionality of the dataset and include only the most informative genes. Given the resulting data matrix with 15150 cells and 4000 genes, we compute a corresponding low-dimensional embedding using PCA. Figure 7 shows the proportion of explained variance of each principal component (PC). We use the first 20 or 30 PCs for predicting population dynamics using `GSBFLOW`. This is in alignment with previous analysis of developmental trajectories which uses 30 PCs ([Schiebinger et al., 2019](#)). The same analysis is executed on the MEFs reprogramming dataset by [Schiebinger et al. \(2019\)](#).

C.2. Lineage Branch Analysis of the Embryoid Body scRNA-Seq Data

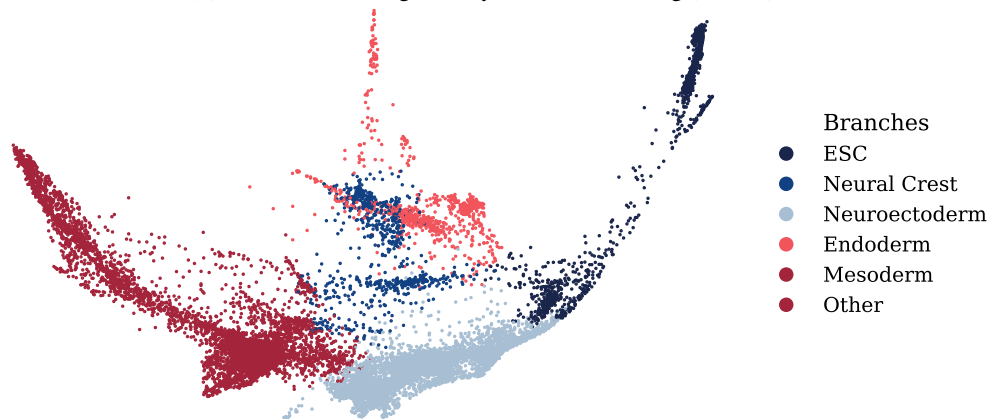
In order to annotate the developmental process and detect lineage branches originating from the differentiation of ESCs, we again follow the analysis of [Moon et al. \(2019\)](#). With a 10-dimensional PHATE embedding of the embryoid body scRNA-seq data (see the first two PHATE components in Fig. 9a), we segment the dataset into 30 clusters using k-means. We then assign the resulting cluster to a lineage subbranch ($i - x$), using the following assignment of subbranch to cluster identification (see Fig. 9b):



(a) PHATE embedding colored by time of snapshot.



(b) PHATE embedding hued by k-Means clustering ($k = 30$).



(c) PHATE embedding hued by predicted lineage branch.

Figure 9. Analysis of embryoid body scRNA-seq data based on PHATE embedding (Moon et al., 2019). Lineage branches are determined based on contiguous k-means clusters.

i. 2, 20	iv. 3, 6, 8, 13, 15, 21, 24	vii. 4, 10, 12, 17, 22	x. 29.
ii. 5, 19	v. 0, 7, 14, 25, 28	viii. 1	
iii. 9, 11, 23	vi. 16, 18, 27	ix. 26	

Then, subbranches are summarized to lineage branches using the assignment in (Moon et al., 2019, Suppl. Note 4):

ESC.	i, ii	Neuroectoderm.	iv	Mesoderm.	vi, vii
Neural Crest.	iii	Endoderm.	v	Other.	viii, ix, x.

The resulting lineage branch annotation of the embryoid body scRNA-seq data can be found in Figure 9c.

D. Experimental Details

In the following, we describe model components, as well as provide details on networks architectures and hyperparameters used.

D.1. The Reference Processes: VE SDEs and sub-VP SDEs

We adopt the VE SDE (Song et al., 2021) as the reference process of the GSB

$$dY_t = g(t) d\mathbb{W}_s, \quad (\text{D.1})$$

where

$$g(t) = \sigma_{\min} \left(\frac{\sigma_{\max}}{\sigma_{\min}} \right)^t \sqrt{2 \log \frac{\sigma_{\max}}{\sigma_{\min}}}.$$

Here, $\sigma_{\min}, \sigma_{\max} \in \mathbb{R}^+$ are two hyperparameters that we sweep for each dataset. The corresponding $q(t)$ in Table 1 is $\sigma_{\min}^2 \left(\frac{\sigma_{\max}}{\sigma_{\min}} \right)^{2t}$, from which one can easily compute all the other functions, and hence (13) as well as (16)-(19).

For existing SB-based methods, we additionally implement the sub-VP SDE (Song et al., 2021), which is determined by a linear function $\beta_t := \beta_{\min} + t(\beta_{\max} - \beta_{\min})$, where as in VE SDE, $\beta_{\min}, \beta_{\max} \in \mathbb{R}^+$ are two hyperparameters that we sweep for each dataset. The reference SDE in (2) is given by

$$c(t) = -\frac{1}{2}\beta_t,$$

$$g(t) = \sqrt{\beta_t \left(1 - e^{-2 \int_0^t \beta_s ds} \right)}.$$

D.2. Network Architectures

Forward and backward policies $Z_t^\theta(x), \hat{Z}_t^\phi(x)$ are time-indexed functions parameterizing the optimal forward and backward drift. Throughout the experiments, we parameterize both $Z_t^\theta(x), \hat{Z}_t^\phi(x)$ via multi-layer perceptrons (MLP). The network architectures change with the complexity of the task. We use four hidden layers of size 128 with sigmoid linear units (SiLU, Swish) as activation function for synthetic data and modeling embryoid body development (Moon et al., 2019). In the MEF reprogramming task (Schiebinger et al., 2019) we apply a MLP with five hidden layers.

D.3. Hyperparameters and Training

For experiments on synthetic data as well as on the task of Schiebinger et al. (2019), we train $Z_t^\theta(x), \hat{Z}_t^\phi(x)$ with batch size 1024. For the task of Moon et al. (2019), we set the batch size to 512. For all experiments, we use the Adam optimizer (Kingma and Ba, 2014) with learning rate $\text{lr} = 0.0002$ ($\beta_1 = 0.5, \beta_2 = 0.9$). Further, we use exponential moving average (EMA) with the decay rate of 0.99.

The hyperparameters of each SDE class, i.e., VE SDE and sub-VP SDE are chosen based on the underlying dataset. On synthetic data, we set $\sigma_{\max} = 2$ in (D.1), for the single-cell tasks we use $\sigma_{\max} = 10$. For sub-VP SDE we set $\beta_{\max} = 4$ in synthetic data setting, and $\beta_{\max} = 20$ in single-cell experiments. In all experiments, we assume a continuous time variable t .

E. Reproducibility

The code will be made public upon publication of this work.